Geosci. Model Dev. Discuss., https://doi.org/10.5194/gmd-2018-277
Manuscript under review for journal Geosci. Model Dev.
Discussion started: 6 December 2018

Geoscientific Model Development Discussions

BARRA v1.0: The Bureau of Meteorology Atmospheric high-resolution Regional Reanalysis for Australia

Chun-Hsu Su[1], Nathan Eizenberg[1], Peter Steinle[1], Dörte Jakob[1], Paul Fox-Hughes[2], Christopher J. White[3,4], Susan Rennie[1], Charmaine Franklin[1], Imtiaz Dharssi[1], Hongyan Zhu[1]

[1] Bureau of Meteorology, Docklands, Victoria 3008, Australia
[2] Bureau of Meteorology, Hobart, Tasmania 7000, Australia
[3] Department of Civil and Environmental Engineering, University of Strathclyde, Glasgow, Scotland, UK
[4] Antarctic Climate and Ecosystems Cooperative Research Centre, Hobart, Australia

Correspondence to: C.-H. Su (chunhsu.su@bom.gov.au)

Abstract. The Bureau of Meteorology Atmospheric high-resolution Regional Reanalysis for Australia (BARRA) is the first atmospheric regional reanalysis over a large region covering Australia, New Zealand and southeast Asia. The production of the reanalysis with approximately 12 km lateral resolution – BARRA-R – is well underway with completion expected in 2019. This paper describes the numerical weather forecast model, the data assimilation methods, and the forcing and observational data used to produce BARRA-R, and analyses results from the 2007-2016 reanalysis. BARRA-R provides a realistic depiction of the meteorology at and near the surface over land as diagnosed by temperature, wind speed and precipitation. It shows closer agreement with point-scale observations and gridded analysis of observations, than leading global reanalyses. In particular, BARRA-R improves upon ERA-Interim global reanalysis in several areas at point-scale to 25 km resolution. BARRA-R shows reduced negative biases in (point-scale) 10 m wind speed during strong wind periods, reduced biases in (5 km gridded) daily temperature maximum and minimum, and higher frequency of very heavy precipitation days at 5 km and 25 km resolution. Few issues with BARRA-R are also identified; some of which are common in reanalyses, such as biases in 10 m wind, and others that are more specific to BARRA such as grid point storms. Some of these issues could be improved through dynamical downscaling of BARRA-R fields using convective-scale (< 2 km) models.

1 Introduction

Reanalyses are widely used for climate monitoring and studying climate change as they provide spatially complete records of the atmosphere for long periods that are a balance between physical consistency and observations. This is achieved by using data assimilation techniques that produce an observation-constrained model estimate of the atmosphere, by drawing short-term model states towards observations from multiple, disparate sources to form an atmospheric analysis. The use of a physically realistic model enables the estimation of unobserved parameters from the limited and irregularly distributed collection of observed parameters.

Geosci. Model Dev. Discuss., https://doi.org/10.5194/gmd-2018-277
Manuscript under review for journal Geosci. Model Dev.
Discussion started: 6 December 2018

Global-scale reanalyses using global atmospheric circulation models (GCMs) have advanced in quality and quantity during the past two decades (Dee et al., 2014; Hartmann et al., 2013). At present, the available global reanalyses established for the satellite era include the NCEP/NCAR reanalysis at 210 km horizontal resolution (Kalnay et al., 1996), the Japanese 55-year Reanalysis (JRA-55) at 60 km (Ebita et al., 2011), the Modern-Era Retrospective analysis for Research and Applications-2 (MERRA-2) at about 50 km (Gelaro et al., 2017) and the European Centre for Medium Range Weather Forecasts (ECMWF) ReAnalysis Interim (ERA-Interim) at ~79 km (Dee et al., 2011). The latter will be replaced by the new ERA-5 ~31 km reanalysis (Hersbach and Dee, 2016). The global reanalyses have the advantages of providing globally consistent and homogeneous reanalyses, but at the expense of spatial resolution. With resolutions typically greater than 50 km, they cannot account for important subgrid variations in meteorology over heterogeneous terrains and islands, and across irregular coastlines, and other small-scale processes (Mesinger et al., 2006; Randall et al., 2007, and references therein).

To address these shortcomings, the development in global reanalysis has also driven concurrent efforts in statistical approaches and dynamical downscaling (e.g., Dickinson et al., 1989; Fowler et al., 2007; Evans and McCabe, 2013). The latter typically embeds a high-resolution meteorological or regional atmospheric model within a global reanalysis, where effects of small-scale forcing and processes such as convection are modelled. Such development is supported by improvements in non-hydrostatic models that run at high resolution in operational numerical weather prediction (NWP) (e.g., Clark et al., 2016). Regional reanalyses are emerging as a step further in this direction. One of the earliest regional reanalyses was the North America Regional Reanalysis (NARR, Mesinger et al., 2006), and the more recent examples include the Arctic System Reanalysis (Bromwich et al., 2018), and reanalyses for Europe and India (Mahood et al., 2018). In contrast to dynamically downscaled global reanalyses, observations are used in regional reanalyses in the same way as the global ones to reduce model errors in high-resolution simulations (Bollmeyer et al., 2015). The resulting observation-constrained reanalyses are expected to have better representations of frequency distributions, extremes and actual space and time-dependent variability (particularly for near-ground variables). Four such European regional reanalyses were developed by the Swedish Meteorological and Hydrological Institute (SMHI), Météo France, Deutscher Wetterdienst (DWD), and UK Met Office (UKMO) within the (recently concluded) European (EU) Seventh Framework Programme (FP7) Uncertainties in Ensembles of Regional Reanalyses (UERRA) project (Borsche et al. (2015) and therein). The project has produced a range of high resolution (5–25 km) ensemble of regional reanalyses of essential climate variables, and of which, the SMHI's HARMONIE [Hi-Resolution Limited Area Model (HIRLAM) Aire Limitée Adaptation Dynamique Développement International (ALADIN) Regional/Mesoscale Operational NWP in Europe] reanalysis has now entered production for the Copernicus Climate Change Service.

Regional reanalyses provide significant added value to the global counterparts in diverse applications ranging from traditional climate studies to industry applications, including regional climate change assessments that include local impact studies (e.g., Fall et al., 2010) and extreme events reconstruction (e.g., Zick and Matyas, 2015). As the regional reanalyses are generally

produced with high spatial as well as temporal resolution, the extremes of variables at local scales can be quantified more accurately. They can provide an alternative reference to evaluate climate projections (e.g., Ruiz-Barradas and Nigam, 2006; Radic and Clarke, 2011). At the same time, embedded forecast models can be used within the framework of the Coordinated Regional Climate Downscaling Experiment (CORDEX) (Martynov et al., 2013) to produce seamless data, where similar modelling systems produce both historical data and projections to provide a higher level of consistency than otherwise possible. They also offer useful data sets for designing new infrastructure, particularly if they are sufficiently long and relevant in spatial resolution and extent to define likelihood of extremes, and intermittency and covariability of phenomena. For instance, COSMO (Consortium for Small-scale Modeling) 6 km reanalysis has shown the potential to provide realistic sub-daily representations of winds at 10 to 40 m height (Borsche et al., 2016), and to resolve small-scale cloud structures (Bollmeyer et al., 2015). NARR has been used to define a climatology of surface wind extremes (Malloy et al., 2015), and 30-year trends in wind at hub height (Holt and Wang, 2012) over northern America.

To date, while the regional reanalyses exists in North America, Europe and India, no atmospheric regional reanalysis for the Australasian region has been produced. To address this gap, the Bureau of Meteorology Atmospheric high-resolution Regional Reanalysis for Australia (BARRA, Jakob et al., 2017) has been produced. BARRA is the first atmospheric regional reanalysis for the Australasian region, with a domain covering Australia, New Zealand, southeast Asia, and south to the Antarctic ice edge (Figure 1). It is produced by the Australian Bureau of Meteorology (Bureau), in partnership with state fire and governmental agencies across Australia, because of the important advantages it allows for planning and management to reduce risks due to extreme weather events including bushfires. For instance, BARRA will address the lack of accurate climate information on surface wind over large areas of Australia due to the low density of the surface network in remote areas to sufficiently observe high variability in wind. BARRA covers a 28-year period from 1990 to 2017, with possible further extensions back and forward in time. BARRA delivers a whole-of-domain reanalysis (identified as BARRA-R) with approximately 12 km lateral resolution, and additional convective-scale (1.5 km horizontal grid-length) downscaled reanalyses (BARRA-x), nested within BARRA-R, centred on major Australian cities to generate additional high-resolution information needed for local-scale applications and studies. They produce a range of gridded data products over their respective domains at their respective resolutions. These products include a variety of 10 min to hourly surface parameters, describing weather and land-surface conditions, and hourly upper-air parameters covering the troposphere and stratosphere. The fields on standardized pressure levels are generated from vertical interpolation of model-level fields. These products include a variety of surface parameters, describing weather and land-surface conditions, at 10 minutes to hourly time resolution, and upper-air parameters on pressure and model levels covering the troposphere and stratosphere at hourly time resolution. BARRA serves to lay the foundation for future generations of reanalyses at the Bureau and to further develop its capabilities to produce seamless climate information that integrates its observational networks and NWP programme.

Geosci. Model Dev. Discuss., https://doi.org/10.5194/gmd-2018-277
Manuscript under review for journal Geosci. Model Dev.
Discussion started: 6 December 2018

In this paper, we describe the forecast model, data assimilation methods, and the forcing and observational data used to produce BARRA-R in Section 2. Section 3 provides an initial assessment of the reanalysis system over the first ten years 2007-2016, with a focus on analysing the quality at or near the surface; Section 4 concludes with a brief summary of our findings.

2 The BARRA-R reanalysis

The development of BARRA follows from the Bureau's experience in operational (deterministic) NWP forecasting over the Australian region using the Australian Community Climate and Earth-System Simulator (ACCESS)-R system (Bureau of Meteorology, 2010; 2013; Puri et al., 2013), and BARRA-R is produced using the UKMO's UERRA system (based on Jermey and Renshaw, 2016) but without the ensemble component. An ensemble NWP forecast system is currently under development at the Bureau. BARRA-R belongs to a class of reanalyses produced by running a limited-area meteorological forecast model forced with a global reanalysis' boundary conditions but drawn closer to observations via data assimilation. In other words, the forecast model provides the means to infer atmospheric states at locations without observations. This section provides an overview of these components while more technical details are included in the references.

2.1 Forecast model

The Unified Model (UM, Davies et al., 2005) is the grid-point atmospheric model used in BARRA-R and ACCESS. It uses a non-hydrostatic, fully compressible, deep-atmosphere formulation and its dynamical core (Even Newer Dynamics for General atmospheric modelling of the environment, ENDGame) solves the equations of motion using mass-conserving semi-implicit, semi-Lagrangian time-integration methods (Wood et al., 2014). The parametrized sub-grid scale processes include convection, radiation, cloud, microphysics, orographic drag and boundary layer turbulence. The prognostic variables are three-dimensional wind components, virtual dry potential temperature and Exner pressure, dry density, and mixing ratios of moist quantities. The grid discretization uses a horizontally staggered Arakawa C-grid (Arakawa and Lamb, 1977) and a vertically staggered Charney-Phillips grid (Charney and Phillips, 1953). The staggered arrangement of grid points allows for accurate finite differencing but results in different model fields located on staggered grids displaced by half a grid spacing along both axes. Data has been left on the staggered grids to allow users to apply the most appropriate re-gridding methods suited for given applications. The vertical levels smoothly transition from terrain-following coordinates near the surface, to constant height surfaces in the upper atmosphere (Davies et al., 2005).

BARRA-R uses version 10.2 of UM and is configured with 70 vertical levels extending from near the surface to 80 km above sea level: 50 model levels below 18 km, and 20 levels above this. While configured with this height based on ACCESS-R, we have more confidence in the data up to a height of 25-30 km where we have most information from observations. The horizontal domain of BARRA-R spans from 65.0° to 196.9° E, -65.0° to 19.4° N (Figure 1), with constant latitude and longitude increments of 0.11° × 0.11° (approximately 12 km) and 1200 × 768 grid points in the horizontal. The model was run to produce

12-hour (12h) forecasts in each 6-hourly cycle (see Section 2.2) to give extra data for the aforementioned dynamical downscaling within the domain.

The parametrizations of sub-grid scale processes (in convection, surface, boundary layer and mixed-phase clouds) in BARRA-R are inherited from the UKMO Global Atmosphere (GA) 6.0 configurations described in Walters et al. (2017a). The GA configurations are also suited for limited-area models with resolutions > 10 km. Several modifications have been implemented,

i. A variable Charnock coefficient is used in surface heat exchange over the sea to improve the tropical Pacific air-sea exchange (Ma et al., 2015).
ii. The heat capacity of "inland water canopy" is set to 2.11×10^{7} J $K^{-1}m^{-2}$ for modelling lakes, which improves diurnal cycle over the inland waters. By contrast, grid cells containing salt lakes in Australia are modelled as bare soil surface (for Lake Eyre and Lake Frome) and vegetated surface (e.g., Lake Lefroy, Lake Ballard).
iii. For its deep convective mass flux scheme, a grid-box dependent convective available potential energy (CAPE) closure scheme is chosen to limit the role of parameterized convection. When vertical velocity exceeds the given threshold of 1 m/s, the vertical velocity dependent CAPE closure is chosen to release the convective instability efficiently (Zhu and Dietachmayer, 2015). These aim to improve the model stability.
iv. The river routing scheme has been turned off because it is not designed for a limited-area model. Therefore, there is no routing of runoff from inland grid points out to sea and inland water bodies, and soil moisture is not affected by this hydrological process.

The characteristics of the lower boundary, climatological fields and natural and anthropogenic emissions are specified using static ancillary fields. These are created as per Walters et al. (2017a, Table 1), with the exceptions of land-sea mask and canopy tree heights. The land-sea mask is created from the 1 km resolution International Geosphere–Biosphere Programme (IGBP) land cover data (Loveland et al., 2000), and the canopy tree heights are derived from satellite light detection and ranging (LiDAR, Simard et al., 2011; Dharssi et al., 2015). Climatological aerosol fields (ammonium sulphate, mineral dust, sea salt, biomass burning, fossil-fuel black carbon, fossil-fuel organic carbon, and secondary organic (biogenic) aerosols) are used to derive the cloud droplet number concentration. Absorption and scattering by the aerosol are included in both the shortwave and longwave.

2.1.1 Land surface

The Joint UK Land Environment Simulator (JULES, Best et al., 2011) is the physically-based land surface component of the UM. It models partitioning of rainfall into canopy interception, surface runoff and infiltration, and uses the Richards' equation and Darcy's law to model soil hydrology. Sub-grid scale heterogeneity of soil moisture is represented by the Probability Distributed Moisture (PDM) model (Moore, 2007). A tile approach is used to represent sub-grid scale heterogeneity in land

cover, with the surface of each land point subdivided into five vegetation types (broadleaf tree, needle-leaved trees, temperate C3 grass, tropical C4 grass and shrubs) and four non-vegetated surface types (urban, inland water, bare soil and land ice). It describes a 3 m soil column with a 4-layer soil scheme with soil thicknesses of 0.1, 0.25, 0.65 and 2.0 m, and models vertical heat and water transfer within the column with van Genuchten hydraulic parameters. The JULES urban parameters are optimised for Australia as described by Dharssi et al. (2015).

2.1.2 Soil moisture

For the 1990 to 2014 period, soil moisture fields in BARRA-R are initialised daily at every 06 UTC using soil moisture analyses from an offline simulation of JULES, at 60 km resolution, driven by bias corrected ERA-Interim atmosphere forcing data, using methods described in Dharssi and Vinodkumar (2017) and Zhao et al. (2017). For 2015 and onward, soil moisture fields in BARRA are initialised daily at every 06 UTC using 40 km resolution soil moisture analyses from the Bureau's global NWP system – ACCESS-G (Bureau of Meteorology, 2016). These external soil moisture analyses are downscaled to the BARRA-R grid using a simple method that takes into account differences in soil texture. The daily initialisation was conducted with the purpose of avoiding spurious drift in the BARRA moisture fields. As well, in each 6-hourly cycle, a land surface analysis is conducted within BARRA (see Section 2.2).

2.1.3 Boundary conditions

The BARRA-R sequential data assimilation process is initialized using ERA-Interim analysis fields (see Sec. 2.2), after which the only relationship with ERA-Interim is solely through the lateral boundary conditions. Hourly lateral boundary conditions for BARRA-R are interpolated from ERA-Interim's 6-hourly analysis fields at 0.75° × 0.75° resolution. The rim width of the boundary frame is 0.88°.

The land boundary is provided by a land surface analysis (Sec. 2.2). Daily sea-surface temperature (SST) and sea ice (SIC) analysis at 0.05° × 0.05° resolution from reprocessed (1985-2007, Roberts-Jones et al., 2012) and near real-time (NRT) Operational Sea Surface Temperature and Ice Analysis (OSTIA, Donlon et al., 2012) are used as lower boundaries over water after being interpolated to the UM grid. The NRT data is used from January 2007. OSTIA is widely used by NWP centres and operational ocean forecasting systems, owing to their short real-time latency. Even though the re-processed and NRT data do not constitute a homogeneous timeseries, OSTIA is favoured over other SST reanalyses owing to its higher spatial resolution. Masunaga et al. (2015, 2018) have shown steep SST gradients, unresolved by coarse SST reanalyses, can influence the organization of long-lived rain bands and enhancement or reduction of surface convergence, and this is particularly problematic for atmosphere-only reanalyses as thermal structure and motions in the marine atmospheric boundary later are not well constrained by data assimilation.

Geosci. Model Dev. Discuss., https://doi.org/10.5194/gmd-2018-277
Manuscript under review for journal Geosci. Model Dev.
Discussion started: 6 December 2018

2.2 Data assimilation system

The BARRA-R analysis scheme is based on fixed deterministic atmospheric and land surface assimilation systems used by UKMO for its UERRA reanalysis (Jermey and Renshaw, 2016) and in the Indian Monsoon Data Assimilation and Analysis (IMDAA) reanalysis (Mahmood et al., 2018). BARRA-R uses a sequential data assimilation scheme, advancing forward in time using 6-hourly analysis cycles centred at synoptic hours t_0 = 0, 6, 12 and 18 UTC, and 12h forecast cycles from t_0-3h (Figure 2). As noted before, longer-range forecasts are needed for driving the downscaling models.

In each analysis cycle, available observations, distributed across a 6h analysis window t_0-3h ≤ t < t_0+3h, are combined with the prior information of the model forecast from the previous cycle (known as the background state), to provide a more accurate estimate of the atmosphere over this window. This first involves a 4-dimensional variational (4DVar) analysis of the basic upper-air atmospheric fields (wind, temperature, specific humidity, pressure) with conventional and satellite observations (see below). 4DVar is favoured over 3DVar as it takes account of time tendency information in the observations and this has significant positive impact on forecasts (Rawlins et al., 2007). The UKMO's VAR assimilation system (version 2016.03.0) is used. The 4DVar uses a linear perturbation forecast (PF) model (Lorenc 2003; Rawlins et al., 2007, Lorenc and Payne, 2007), which uses a simpler model state linearised about a 'guess' trajectory (i.e., tangent linear model) with a lower resolution (0.33° cf. 0.11°) than the full forecast model. The lower resolution is chosen to limit computational costs. The PF model uses a simplified set of physical parameterizations including a simple boundary layer, cloud latent heat release, large-scale precipitation and convection. In other words, it is assumed that the lower-resolution corrections to the background state (i.e. increments), interpolated to a higher resolution, are suitable corrections for the full model. The analysis increments from 4DVar valid at t_0-3h are added to the background state at t_0-3h to produce an improved initial condition for the forecast model to perform the next 12h forecast from t_0-3h to t_0+9h. A constraint of zero analysis increments is specified at the model boundary such that BARRA-R relies on the driving model ERA-Interim to define large-scale flow and other atmospheric conditions.

The variational method of assimilation minimises a cost function whose two principal terms penalise distance to the background state and distance to the observations. The two terms are squared differences weighted by the inverse of their corresponding error covariances. In BARRA-R, the background error covariance has been estimated by a smooth parameterised approximation to climatology tuned by forecast differences (Ingleby, 2001). Accordingly, the estimated background error covariance is invariant between successive analysis windows, but is time varying within the analysis window. The cost function also includes a pressure-based energy norm that serves as a weak constraint digital filter to suppress spurious fast oscillations associated with gravity-inertia waves produced in model forecasts when analysis increments are added to the background state (Gauthier and Thépaut, 2001).

The initial land surface state can have a significant impact on short-term forecasts of screen-level temperature and humidity, and the quality of the initial state can also be improved through data assimilation. An Extended Kalman Filter (EKF) using

observations of 2 m temperature and humidity is used to analyse the BARRA land state at every 6 hour cycle and provide analyses of soil moisture, soil temperature and skin temperature as described by Dharssi et al. (2012). The assimilation of satellite microwave retrieved soil moisture is not attempted here as it has not been implemented in ACCESS. The UKMO's SURF analysis system (version 2016.07.0) is used to perform EKF. The Jacobian, which relates observed variables to model variables, for the Kalman gain matrix is estimated using finite difference by perturbing each model variable to be analysed in 40 perturbations and performing short 3-hour forecasts. Here JULES (version 3.0) is run in the standalone mode, decoupled from the UM. The BARRA land state is reconfigured with EKF-derived surface analyses at every t_0.

Notice that the last 6h forecast of this model run represents the prior state estimates needed for the next analysis cycle. The forecast fields valid at t_0-3h, t_0-2h and t_0-1h are discarded, as these fields may still be influenced by transient artefacts due to the slight imbalance introduced by the addition of the analysis increments. It is already noted that this effect is mitigated with the energy norm in the 4DVar's cost function that penalises the unbalanced structure in the increments.

The reanalysis is produced with multiple parallel production streams to speed up production. Each stream has a month of spin-up time from the ERA-Interim initial conditions before production data is archived. Trials undertaken at the Met Office have shown that a one-month period is sufficient for spin-up (Renshaw et al., 2013). Most streams are set up to produce one year of reanalyses, excluding the first month of spin-up.

2.3 Observations

Conventional (namely, land surface stations, ships, drifting buoys, aircrafts, radiosondes, wind profilers) and satellite (retrieved wind, radiances and bending angle) observations are assimilated in BARRA-R. The various observational types are chosen as they have been assimilated in the Bureau's operational NWP systems; other observational types, such as clear-sky radiances, have not been assimilated due to time constraint to set them up. Rain observations from radar and gauges are not assimilated as their assimilation schemes are still being tested for operational NWP. As listed in Table 1, the data sets are taken from multiple sources, as they are being prepared during the production runs. Most of the observations prior to 2003 are supplied by ECMWF, and those between 2003 to 2009 and conventional data from 2003 are extracted from the UKMO operational archives.

The Bureau's archived observational data is also used to support this work. We assimilate additional high frequency (10 min) land surface observations from automatic weather stations in Australia, and locally derived satellite atmospheric motion vectors (AMV). All the satellite data from 2010 onwards is taken from the Bureau's operational archives. Ground positioning system (GPS) radio occultation bending angle data up to 2009 is provided by the Radio Occultation Meteorology Satellite Application Facility (ROM SAF) and is extracted from the Bureau's archives for the time period since 2010. Additional land surface

observations over New Zealand are extracted from their National Climate Database (CliFlo, 2017). The 4DVar assimilation of local AMV (Le Marshall et al., 2013) and GPSRO (Le Marshall et al., 2010) has been shown to improve operational forecasts.

Before being assimilated, observations are screened to select best quality observations, remove duplicates and reduce data redundancy via thinning, using the UKMO's OPS system (based on version 2016.03.0). There are per-cycle quality controls performed based on the method of Lorenc and Hammon (1988). Observations significantly different from the model background are rejected when exceeding a threshold calculated by a Bayesian scheme, unless they are consistent with other observations nearby. The observational error variances and thinning distances are established at the UKMO and the Bureau for their NWP systems. For the surface, sonde and aircraft observations, an observation automatic monitoring system performs monthly blacklisting of sites that show consistently large differences with BARRA-R's forecast over a one-month period. The system also calculates bias corrections for surface pressure and for aircraft and sonde temperature.

For the satellite data, instruments and their individual channels are rejected when they become unreliable. The blacklisting is informed by the work of ECMWF and MERRA2 reanalysis teams for their reanalyses. Further, airmass-dependent variational bias correction is applied to satellite radiances as part of the assimilation process, allowing the time-varying corrections to fit drifts in instrumental bias (Harris and Kelly, 2001; Dee and Uppala, 2008). The bias corrections were calculated monthly, with the satellite radiances during the first month of each production stream not assimilated. There are abrupt changes to the amount of satellite data assimilated at the start and end of satellite missions and the various observational data archives; in some cases, abrupt changes occur when corrections were made to the observation screening and thinning rules mid-production of the 2010-2015 reanalyses. The impacts of these are still to be investigated.

3 Preliminary evaluation of ten-year regional reanalysis

3.1 Analysis departure statistics

The observation departure statistics of the analysis can be compared against those of the model background state (Sec. 2.2) to indicate how closely the reanalysis fits the observational data before and after an analysis cycle. Root-mean-squared difference (RMSD) and additive bias (bias, for brevity) are used to measure the departures for a wide range of observed fields, where bias is calculated as $E(d_m) - E(d_o)$, where $E(*)$ yields the expectation in time, d_m refers to the timeseries of model values and d_o are the observed values. Table 2 reports the ten-year mean values of the RMSD and bias for surface, sonde, aircraft-based and satellite wind fields. The assimilation process is behaving as desired by drawing the model towards the observations by reducing the RMSD and the magnitude of the bias for nearly all observational types. Monthly timeseries of the departure statistics, shown in the Supplementary Material, also suggests that this is achieved across the period.

Geosci. Model Dev. Discuss., https://doi.org/10.5194/gmd-2018-277
Manuscript under review for journal Geosci. Model Dev.
Discussion started: 6 December 2018

3.2 Surface

The advantages of BARRA-R over global reanalyses are most likely to be found near the surface, as BARRA-R resolves near-surface features larger than 12 km in scale and assimilates more surface observations over Australia and New Zealand. This section first presents a point-scale evaluation of BARRA-R against surface observations, followed by comparison with gridded climate data.

3.2.1 Point evaluation of 2 m temperature, 10 m wind speed and surface pressure

The t_0+6h model forecasts of screen (2 m) temperature, 10 m wind speed and surface pressure are evaluated against land observations. These forecasts have some independence from the observations as they are not used in the analysis of the associated cycle t_0. Since errors tend to grow with the forecast range, the assessment estimates an upper bound on the true errors of the analysis fields between time t_0 and t_0+3h. These fields are interpolated between the model's model levels using surface similarity theory (Walters et al., 2017a). The ERA-Interim t_0+6h forecasts are also evaluated to serve as a benchmark, where its forecasts are performed twice daily from 0 and 12 UTC. It is not ideal to directly compare two reanalyses with different resolutions, and interpolating them onto common observed locations before evaluation diminishes some of the improvement achieved by BARRA-R relative to ERA-Interim. Nonetheless, we undertake the latter to assess whether the models contain information at the higher scale information captured by point measurements; it therefore does not provide an assessment of the true quality of the models at their native resolutions.

To correct representativity errors in both reanalyses, their model fields at (modelled) land points are interpolated to the observation times and the station locations via bilinear interpolation in time and in the horizontal direction. Height corrections are applied to the interpolated fields to match the station heights: the corrections to the screen temperature is based on dry adiabatic lapse rate (Sheridan et al., 2010), 10 m wind speed is based on Howard and Clark (2007), and the correction to surface pressure is based on the hydrostatic equation under a constant lapse rate. As the observations are irregularly distributed in time, we consider all observations within a t_0+5h to t_0+7h time window, with t_0 being 0 and 12 UTC, and the model grids are linearly interpolated to the observation times. RMSD, Pearson's linear correlation, additive bias and variance bias are calculated at each station, with the variance bias being calculated as $Mbias = var(d_m)/var(d_o) - 1$ to capture differences in the dispersion, where $var(*)$ computes the variance in time. The correlation assesses the temporal mismatch between the model and observations.

Figure 3 shows the distribution of scores across 900-1500 stations in the BARRA-R domain in boxplots. BARRA-R shows better agreement with the point observations than ERA-Interim for most surface variables and measures. BARRA-R's screen temperature shows higher correlation and lower biases. BARRA-R shows lower RMSD than ERA-Interim at over 80% of the stations for screen temperature, and at 70% of stations for 10 m wind speed and surface pressure (see Supplementary Material).

At closer inspection, a percentile comparison plot of screen temperature deviation from monthly mean, shown in Figure 4(a), indicates that the frequency distribution of BARRA-R temperature is closer to that of the observations than ERA-Interim, particularly in regimes below 5% percentiles and above 95% percentiles.

For 10 m wind speed, negative biases for variance exist in both reanalyses, but less so for BARRA-R. Figure 4(b) shows that they are positively biased during low wind conditions and vice versa during strong wind speeds. There are many possible reasons for under-estimating strong winds: the inaccurate descriptions of boundary layer mixing and form drag for sub-grid orography, and of surface properties such as land cover and vegetation types. Changing the fractional area of the vegetation canopy modifies scalar roughness of the vegetated tiles, affecting the wind speed. The seemingly linear variation in wind speed is known in the global reanalyses (e.g., Carvalho et al., 2014), and Rose and Apt (2016) attributed the problem of wind underestimation to inaccuracy in modelling wind speeds in unstable atmospheric conditions.

Pressure is a large-scale variable which is likely to be better represented by a global model than a limited-area model, although the BARRA-R estimates of point-scale surface pressure are more accurate in topographically complex regions and coast lines, where ERA-Interim estimates are poor, so that the inter-quartile range of the RMSD scores for BARRA-R is significantly narrower than for ERA-Interim.

3.2.2 Comparisons with gridded analysis of observed temperature

The reanalyses are compared against a gridded daily 0.05° × 0.05° analysis of station temperature data from the Australian Water Availability Project (AWAP, Jones et al., 2007). The AWAP grids are generated using an optimised Barnes successive-correction method that applies weighted averaging of the station data. Topographical information is included by using anomalies from long-term (monthly) averages in the analysis process. Figure 5 shows the ten-year mean in daily maximum and minimum temperature from AWAP, ERA-Interim and BARRA-R. The daily statistics are derived from 3-hourly forecast fields of ERA-Interim and hourly fields of BARRA-R. While inherent biases due to sampling are expected, this comparison distinguishes the advantage of higher frequency data generally found in a regional reanalysis when examining lower and upper tail statistics. The spatial variation in BARRA-R is very similar to AWAP, especially across the eastern seaboard of Australia where Eastern Highlands are the major driver for temperature variability. The insets show the contrasts from AWAP when the reanalyses are downscaled to the AWAP grid. BARRA-R shows cold and warm biases of around 1 K in daily maximum and minimum temperature respectively, particularly over the eastern region. Despite this, BARRA-R shows better agreement than ERA-Interim, which reports differences in mean up to 5 K in magnitude. The reduced amplitude in screen temperature is a long-standing problem in UM; experiments undertaken by UM development partners have shown that changes to the representation of the land surface (e.g., reductions in the amount of bare soil and changes to scalar roughness and albedo of vegetated tiles) reduce clear-sky biases (Bush et al., 2018).

Geosci. Model Dev. Discuss., https://doi.org/10.5194/gmd-2018-277
Manuscript under review for journal Geosci. Model Dev.
Discussion started: 6 December 2018

3.3 Pressure levels

To assess BARRA-R in the atmosphere, we compare the t_0+6h forecasts on pressure levels from BARRA-R with radiosonde and pilot wind observations at 0 and 12 UTC on standard pressure levels, using the harmonized data set produced by Ramella Pralungo et al. (2014a; 2014b). The pressure-level fields of BARRA-R and ERA-Interim's analyses at time t_0 are also compared, even though they are not independent from the observations; such comparisons only provide baselines to interpret the relative quality of the BARRA-R forecasts. Similar comparisons with the ERA-Interim's twice-daily forecasts at these observation times are also not possible because they start from 0 and 12 UTC. The model data is interpolated horizontally to the sonde and pilot launch locations via bilinear interpolation, and the RMSD is calculated at each location.

Evaluations are undertaken at pressure levels ranging from 1000 to 10 hPa, and the resulting boxplots of RMSD are shown in Figure 6. Depending on the pressure level and parameter evaluated, between 54 to 203 sites were available. There is a marked variability in RMSD with the pressure levels, particularly for wind speed, due to a range of reasons such as variations in the number of observing sites, increasing sonde drift error on ascent, and differences in dynamic range of the fields with height. A markedly higher RMSD for wind speed at height of 200 hPa where the jet stream can occur.

It is difficult to discern the differences between the two analyses, suggesting that they perform similarly from assimilating the same observations. Assimilation at a coarser resolution of 0.33° (cf. 0.11° of the forecast model) in BARRA-R does not drastically improve 0.75° representations of temperature and wind at these pressure levels and at point scales. There are also small differences between the analyses and BARRA-R background, indicating that the 0.11° forecast model does not degrade from the lower-resolution analysis of BARRA-R but does also not improve upon the ERA-Interim's 0.75° representation of these fields.

3.4 Precipitation

Rain observations are not assimilated in either BARRA-R or ERA-Interim. Precipitation estimation within the forecast models is constrained by other observations. The UM uses the microphysics scheme based on Wilson and Ballard (1999) to form and evolve precipitation due to grid-scale processes (Walters et al., 2017a). For sub-grid scale processes, it uses a mass flux convective parameterization scheme with the CAPE closure (Gregory and Rowntree, 1990) to produce the convective-scale motion (< 10 km) and thus prevent unstable growth of cloudy structures on the grid (Clark et al., 2016). The latter works independently at each grid point, and the model can only predict the area-average rainfall, instead of the spectrum of rainfall rates. In other words, BARRA-R's precipitation estimates from sub-grid convection processes will be erroneous than those for large-scale precipitation. The accuracy of BARRA-R is expected to poorer during the warm season and at low latitudes, while better during cooler season and at high latitudes where non-convective precipitation is dominant. To allow the UM to spin-up from the 0.33° analysis increments, we examine the quality of the precipitation accumulation between t_0+3h to t_0+9h, by

comparing against gridded data sets. This also addresses the issue that the UM has an excess of precipitation at analysis time (t_0-3h) due to a temporary imbalance in the moisture fields, by allowing time for the model to adjust to remove the excess.

For ERA-Interim, we used its first 12h accumulation because it is considered the most accurate (Kallberg, 2011). We examine BARRA-R and ERA-Interim with 0.05° × 0.05° raingauge analysis of daily accumulation from AWAP and 0.25° × 0.25° satellite-based analysis of 3-hourly rain rates from the Tropical Rainfall Measuring Mission (TRMM) multi-satellite precipitation analysis (TMPA 3B42 version 7, Huffman et al., 2006). The AWAP rain grids are also produced using the same Barnes method, where the ratio of observed rainfall to monthly average is used in the analysis process. Some areas in AWAP have been masked (shown in white) because there were insufficient observations to derive reliable estimates. There are limitations in comparing datasets with different grids. Specifically, products with coarser grids tend to over-represent low-threshold events occurring at spatial scales smaller than their native grid sizes and under-represent high-threshold events.

The first column in Figure 7 compares the ten-year annual mean precipitation amount estimated from the four data sets. BARRA-R provides a realistic depiction when compared with TMPA across the domain, showing high precipitation over the tropics and over the Tasman Sea and Southern Ocean. By contrast, ERA-Interim shows even higher precipitation over the tropics and insufficient rain over the Tasman Sea. TMPA is expected to be less accurate over the ocean due to the absence of local observations used for gauge adjustments (Sapiano and Arkin, 2009), and south of 40°S due to limited local cross-sensor calibration (Huffman et al., 2008). BARRA-R also agrees very well with AWAP over Australian land areas, reflecting the markedly higher precipitation in the northern tropics, and western Tasmania. Notice the discrepancy between AWAP and TMPA over Tasmania, suggesting possible negative biases in TMPA in high-latitude regions with significant topography due to difficulties of satellite retrievals over snow covered surfaces and/or due to the high elevations where TMPA often underestimates precipitation (Barros et al. 2006; Matthews et al. 2013). BARRA-R also shows better agreement in some of the dry areas such as western Australia.

The frequency of days with three intensity regimes is examined next. First, we examine the frequency of light rain days with amount between [1,10) mm, with the 1 mm threshold being chosen. This accounts for the tendency of the model to create light "drizzle" events with very low rain rates. Comparing with TMPA, the two reanalyses tend to show significantly more rain days in the tropics, western Tasmania, and the Southern Ocean. TRMM is known to miss amount of light rainfall and drizzle over subtropical and high-latitude oceans (Berg et al., 2010), while simulated precipitation over the Southern Ocean over-estimates drizzle (Franklin et al., 2013; Wang et al., 2015) when compared with satellite observations. Some of these differences from TMPA are not mirrored by AWAP over Australia, suggesting possible under-estimation of rain days in TMPA over land where the gauge network is relatively dense (see Supplementary Material). Despite these considerations, BARRA-R over-estimates the frequency of light rain days when compared with AWAP, notably in the northern and central regions of Australia, and Tasmania. The UM's parameterized convection scheme assumes that there are many clouds per grid box – which is marginal

at the BARRA-R's resolution, and thus produces a bias towards widespread precipitation and has little indication of the areas which could expect larger rain rates (Clark et al., 2016).

For heavy precipitation days, with amount [10,50) mm, there are greater similarities between BARRA-R and AWAP, over regions such as southeast coast of Australia and Tasmania, than for ERA-Interim. However, BARRA-R underestimates the frequency over Australia north of 30°S. Over the ocean, the two reanalyses show more heavy precipitation days than TMPA, although BARRA-R is more similar to TMPA.

Finally, for the very heavy precipitation days (≥ 50mm), it is obvious that ERA-Interim does not capture enough frequency over land in northern Australia, and southeast Asia, whereas BARRA-R is more comparable with AWAP and TMPA. This agrees with the findings of Jermey and Renshaw (2016) that higher-resolution regional reanalyses show improvement in representing high-threshold events at these spatial scales. Over the land in northern Australia, there are discernible differences in spatial variability between AWAP and BARRA-R. Over the ocean, BARRA-R also shows greater rainfall intensity in the tropics than ERA-Interim, but both reanalyses show lower intensity compared to TMPA. Since satellite-derived estimates of convective precipitation are largely accurate in the low latitudes (Ebert et al., 2007, Chen et al., 2013), these reflect the deficiency of the parameterized convection scheme in BARRA-R for estimating convective precipitation in this region.

Figure 8 compares domain-averaged monthly totals of the reanalyses with TMPA, on the TMPA grid over five sub-domains. Precipitation over land and ocean are distinguished. BARRA-R shows good agreement with ERA-Interim and TMPA for tropical, subtropical and temperate regions between 39.2° to 10.0° South. BARRA-R shows significantly higher totals between ±10° over land, owing to occurrences of "grid-point storms". These can occur over high or sharp topographical regions, such as in Papua New Guinea, and Indonesia, and Pacific islands resolved only as single or few 0.11° × 0.11° cells. Numerical noise during computations can accumulate to trigger a fictitious storm by the convective parameterization scheme. The condensation heat release at the saturated grid box leads to a strong uplift. The model then removes this excess moisture in the column by generating very large precipitation localised at that grid cell. This is more likely to occur over land in the tropics and sub-tropics and during the warm seasons, when the atmosphere is unstable and there is sufficient warm moisture supply at the surface.

BARRA-R also shows higher monthly totals below 39.2° South latitude over Tasmania and New Zealand, than TMPA and ERA-Interim. The discrepancy is partly due to (aforementioned) negative bias in TMPA and ERA-Interim in Tasmania, and occurrences of grid-point storms in BARRA-R over its high topography in New Zealand.

Geosci. Model Dev. Discuss., https://doi.org/10.5194/gmd-2018-277
Manuscript under review for journal Geosci. Model Dev.
Discussion started: 6 December 2018

4 Summary and outlook

BARRA represents one of the latest global efforts to develop regional reanalyses, and is the only one to date that focuses on the Australasian section of the Southern Hemisphere. It is developed with significant co-investment from state-level emergency service agencies across Australia, due to the advantages of deeper understanding of past weather, including extreme events, and especially in areas that are currently poorly served by observation networks. BARRA will ultimately represent a collection of high-resolution gridded meteorological data sets with 12 km and 1.5 km lateral spatial resolution and 10 minutes to hourly time resolution. The production is well underway and is expected to complete in 2019.

In this paper, we describe the BARRA 12 km regional reanalysis, which is closely related to the Bureau's regional NWP system, although with an updated UM, 4DVar (with variational bias correction) and automated station blacklisting systems are used. BARRA-R covers a significant region of the globe including parts of South East Asia and the eastern Indian Ocean, the southwest Pacific, Australia and New Zealand and assimilates a wide range of conventional and satellite observations that have proven to improve the skill of NWP.

BARRA-R produces a credible reproduction of the meteorology at and near the surface over land as diagnosed by the selected variables. BARRA-R improves upon its global driving model, ERA-Interim, showing better agreement with point-scale observations of 2 m temperature, 10 m wind speed and surface pressure. Daily maximum and minimum statistics for 2 m temperature at 5 km resolution are captured in BARRA-R with smaller biases than ERA-Interim. BARRA-R's 10 m wind fields show lower biases than ERA-Interim, but the negative bias during strong winds, which is common amongst other reanalyses, remains significant. This bias could be addressed via post-processing using methods such as that of Rose and Apt (2016). Altogether, BARRA-R provides better representation of near-surface extremes, which has implications for its uses for energy management, fire risk and storm damages. Our study did not discern clear merits in BARRA-R analysis and forecast, relative to ERA-Interim analysis, for the pressure-level temperature and wind. Other evaluations of the GA6 configurations including tropical cyclones, precipitation, clouds and large-scale flow, are reported in Walters et al. (2017a; 2017b), albeit in global models at coarser spatial resolutions.

Precipitation fields from BARRA-R show similarities with AWAP's gridded daily raingauge analysis over Australia, where it reflects more similar frequency statistics for heavy rain events and annual mean than ERA-Interim. While this is expected from comparing grids with different measurement support, BARRA-R is expected to contain more information pertaining to rain events at local scales. The frequency statistics (of both light and heavy rain days) of the two reanalyses are markedly different from TMPA over regions exterior to Australia, even though the variability of the monthly totals is very similar amongst the reanalyses and TMPA across the domain. BARRA-R is likely to be positively biased over land in the regions north of 10° S and New Zealand due to grid-point storms, but the likely TMPA precipitation underestimations associated with the high elevations make this difficult to quantify through direct comparison. The disagreement with TMPA is also apparent

over the oceans, but consensus between satellite-based products generally degrades over higher latitudes, especially over the southern oceans (Behrangi et al., 2014). The distinct characteristics of grid-point storms in terms of superficial spatial localization, precipitation amount and vertical wind speed, could be detected and screened out via post-processing. More in-depth evaluation of BARRA-R precipitation estimates against point gauge observations and AWAP are reported in Acharya et al. (2018).

Higher resolution models used to downscale BARRA-R would also alleviate these shortcomings by resolving sharp topographical features, resolving sub-grid processes (e.g., convection), and using science configurations more suited for a given climatic region. Assessment of the UM's first Regional Atmosphere (RA1) science configurations for convective-permitting models, recently concluded in December 2017, distinguishes two different science configurations for mid-latitude and tropical regions (RA1-M and RA1-T respectively). RA1 can lead to improvements to 2 m temperature, 10 m wind speed and precipitation (Bush et al., 2018). Further, it is known that BARRA-R's convection scheme, involving instantaneous adjustment of cloud fields to changes in forcing (e.g., solar heating), can lead to unrealistic behaviour at places such as coasts and in time (e.g., incorrect diurnal cycle) (Clark et al., 2016). A companion article will examine the relative merits between downscaled regional reanalyses and BARRA-R.

The recent development of the global and regional reanalyses addresses the need for high-quality, increasingly higher resolution, and longer-term reanalyses, accompanied by uncertainties, within the research and broader user communities. BARRA therefore represents the recent effort in the development of regional reanalyses, and is the first to focus on the Australasian region. It is developed with significant co-investment from state-level emergency service agencies across Australia, due to the advantages of deeper understanding of past weather, including extreme events, and especially in areas that are currently poorly served by observation networks. The 28-year BARRA reanalysis, which is expected to be completed fully in 2019, will ultimately represent a collection of high-resolution gridded meteorological data sets with 12 km and 1.5 km lateral spatial resolution and 10 minutes to hourly time resolution.

BARRA also represents an important step in supporting the Bureau's ability to prepare for future reanalysis-related activities such as data rescue and reprocessing of observational data. Future reanalyses could use higher resolution models and ensemble-based forecast and assimilation systems to quantify uncertainties. They will also benefit from international efforts in reprocessing historical conventional and satellite observations with enhanced quality and/or more accurate uncertainty estimates.

Code availability. All code, including the UM (version 10.2), VAR (version 2016.03.0), JULES (version 3.0), OPS (version 2016.03.0), SURF (version 2016.07.0) systems, used to produce BARRA is version-controlled under Met Office Science Repository Service. Readers are referred to https://code.metoffice.gov.uk/trac/home for access information.

Data availability. The first release of BARRA-R data set for period 2010-2015 is available for academic use, with subsequent releases planned for late 2018 and early 2019. Readers are referred to http://www.bom.gov.au/research/projects/reanalysis for information on available parameters and access.

Competing interests. The authors declare that they have no conflict of interest

Author contribution. PS, DJ, PFH and CJW conceived and/or designed BARRA. CHS, NE and PS developed the BARRA system with inputs from SR, CF, ID and HZ. CHS and NE performed the production and evaluation. CHS prepared the manuscript with contributions from all co-authors.

Acknowledgements

Funding for this work was provided by emergency service agencies (New South Wales Rural Fire Service, Western Australia Department of Fire and Emergency Services, South Australia Country Fire Service, South Australia Department of Environment, Water and National Resources) and research institutions (Antarctic Climate and Ecosystems Cooperative Research Centre (ACE CRC) and University of Tasmania). Funding from Tasmania is supported by the Tasmanian Government and Australian Government, provided under the Tasmanian Bushfire Mitigation Grants Program.

BARRA-R is set up with assistance from the UKMO's UERRA reanalysis team (R. Renshaw, P. Jermey, J. Davis) and colleagues (A. Maycock, D. Walters, I. Boutle), and many colleagues at the Bureau of Meteorology (T. Le, I. Bermous, L. Rikus, C. Sanders, J. Lee, G. Dietachmayer, J. Le Marshall, X. Sun, G. Kociuba, C. Tingwell, H. Zhang), the Commonwealth Scientific and Industrial Research Organisation (CSIRO, M. Dix), National Computational Infrastructure (NCI, D. Roberts). We thank S. Moore and T. Carey-Smith at National Institute of Water and Atmospheric Research (NIWA) for providing additional local observations over New Zealand; R. Smalley on his advice on AWAP; P. May, E. Ebert, and A. Dowdy for their feedback on early drafts of manuscript. BARRA-R uses the ERA-Interim data, provided through ARC Centre of Excellence for Climate System Science (P. Petreli) at NCI. Many of the observational data sets were provided by ECMWF, UKMO and NIWA. The radio occultation data were provided by the Radio Occultation Meteorology Satellite Application Facility (ROM SAF, through K. B. Lauritsen) which is a decentralized operational RO processing center under EUMETSAT. RO data are available at http://www.romsaf.org. This project was undertaken with the assistance of resources and services from NCI, which is supported by the Australian Government.

ERA-Interim can be retrieved from ECMWF, https://www.ecmwf.int/en/forecasts/datasets/archive-datasets/reanalysis-datasets/era-interim. AWAP data can be requested from, http://www.bom.gov.au/climate, and TMPA v7 data is retrieved via NASA Goddard Earth Sciences (GES) Data and Information Services Center (DISC), https://disc.gsfc.nasa.gov/datasets/TRMM_3B42_V7/summary.

References

Acharya, S. C., Nathan, R., Wang, Q. J., Su, C.-H., and Eizenberg, N.: An evaluation of daily precipitation from atmospheric reanalysis products over Australia, in preparation.

Arakawa, A., and Lamb, V. R.: Computational design of the basic dynamical processes of the UCLA general circulation model. Methods of Comp. Phys.: Adv. Res. Appl., 17, 173–265, doi: 10.1016/B978-0-12-460817-7.50009-4, 1977.

Barros, A. P., Chiao, S., Lang, T. J., Burbank, D., and Putkonen, J.: From weather to climate—Seasonal and interannual variability of storms and implications for erosion process in the Himalaya. Geological Society of America Spatial Paper 398, Penrose Conference Series, 17–38, 2006.

Behrangi, A., G. Stephens, R.F. Adler, G.J. Huffman, B. Lambrigtsen, and M. Lebsock: An update on the oceanic precipitation rate and its zonal distribution in light of advanced observations from space. J. Climate, 27, 3957–3965, doi: 10.1175/JCLI-D-13-00679.1, 2014.

Berg, W., T. L'Ecuyer, and J.M. Haynes: The distribution of rainfall over oceans from spaceborne radars. J. Appl. Meteor. Climatol., 49, 535–543, doi: 10.1175/2009JAMC2330.1, 2010.

Best, M.J., Pryor, M., Clark, D.B., Rooney, G.G., Essery, R.L.H., M´enard, C.B., Edwards, J.M., Hendry, M.A., Porson, A., Gedney, N., Mercado, L.M., Sitch, S., Blyth, E., Boucher, O., Cox, P.M., Grimmond, C.S.B. and Harding, R.J.: The Joint UK Land Environment Simulator (JULES), model description - Part 1: Energy and water fluxes. Geosci. Model Dev., 4(3) 677–699. doi:10.5194/gmd-4-677-2011, 2011.

Bollmeyer, C. , Keller, J. D., Ohlwein, C. , Wahl, S. , Crewell, S. , Friederichs, P. , Hense, A. , Keune, J. , Kneifel, S. , Pscheidt, I. , Redl, S. and Steinke, S.: Towards a high-resolution regional reanalysis for the European CORDEX domain. Q. J. R. Meteorol. Soc., 141: 1-15. doi:10.1002/qj.2486, 2015.

Borsche, M., Kaiser-Weiss, A. K., Unden, P., and Kaspar, F.: Methodologies to characterize uncertainties in regional reanalyses. Adv. Sci. Res., 12, 207-218, doi: 10.5194/asr-12-207-201, 2015.

Borsche, M., Kaiser-Weiss, A.K., and Kaspar, F.: Wind speed variability between 10 and 116 m height from the regional reanalysis COSMO-REA6 compared to wind mast measurements over Northern Germany and the Netherlands. Adv. Sci. Res., 13, 151–161, doi: 10.5194/asr-13-151-2016, 2016.

Bromwich, D., A. Wilson, L. Bai, Z. Liu, M. Barlage, C. Shih, S. Maldonado, K. Hines, S.-H. Wang, J. Woollen, B. Kuo, H. Lin, T. Wee, M. Serreze, and J. Walsh: The Arctic System Reanalysis Version 2. Bull. Amer. Meteor. Soc., 99, 805-828, doi: 10.1175/BAMS-D-16-0215.1, 2018.

Bureau of Meteorology: Operational implementation of the ACCESS numerical weather prediction systems, NMOC Op. Bull. No. 83, accessed online, http://www.bom.gov.au/australia/charts/bulletins/apob83.pdf, 2010.

Bureau of Meteorology: APS1 upgrade of the ACCESS-R numerical weather prediction system, NMOC Op. Bull. No. 98, accessed online, http://www.bom.gov.au/australia/charts/bulletins/apob98.pdf, 2013.

Bureau of Meteorology: APS2 upgrade to the ACCESS-G numerical weather prediction system, BNOC Op. Bull. No. 105, accessed online, http://www.bom.gov.au/australia/charts/bulletins/APOB105.pdf, 2016.

Bush, M., et al.: The Met Office Unified Model Regional Atmosphere 1 and JULES Regional Land 1 configurations, in prep., 2018.

Carvalho, D., Rocha, A., Gomez-Gesteira, M., and Santos, C. S.: WRF wind simulation and wind energy production estimates forced by different reanalyses: comparison with observed data for Portugal, Appl. Energy, 117, 116-126, doi: 10.1016/j.apenergy.2013.12.001, 2014.

Charney, J. G, and Phillips, N. A.: Numerical integration of the quasi-geostrophic equations for barotropic and simple baroclinic flows. J. Meteorol. 10: 71–99, doi: 10.1175/1520-0469(1953)010<0071:NIOTQG>2.0.CO;2, 1953.

Chen, Y., E. E. Ebert, K. J. E. Walsh, and N. E. Davidson: Evaluation of TRMM 3B42 precipitation estimates of tropical cyclone rainfall using PACRAIN data, J. Geophys. Res. Atmos., 118, 2184-2196, doi: 10.1002/jgrd.50250, 2013.

Clark, P., Roberts, N., Lean, H., Ballard, S. P., and Charlton-Perez, C.: Review: Convection-permitting models: a step-change in rainfall forecasting, Meteor. App., 23, 165–181, doi: 10.1002/met.1538, 2016.

CliFlo: NIWA's National Climate Database on the Web, http://cliflo.niwa.co.nz, Data Retrieved: 17 February 2017.

Davies, T., Cullen, M. J. P., Malcolm, A. J., Mawson, M. H., Staniforth, A., White, A. A., and Wood, N.: A new dynamical core for the Met Office's global and regional modelling of the atmosphere, Quart. J. Roy. Meteor. Soc., 131, 1759–1782, doi:10.1256/qj.04.101, 2005.

Dee, D. P., Uppala, S. M., Simmons, A. J., Berrisford, P., Poli, P., Kobayashi, S., Andrae, U., Balmaseda, M. A., Balsamo, G., Bauer, P., Bechtold, P., Beljaars, A. C. M., van de Berg, L., Bidlot, J., Bormann, N., Delsol. C., Dragani, R., Fuentes, M., Geer, A. J., Haimberger, L., Healy, S. B., Hersbach, H., Holm, E. V., Isaksen, L., Kallberg, P., Kohler, M,, Matricardi, M., McNally, A. P., Monge-Sanz, B. M., Morcrette, J. J., Park, B. K., Peubey, C., de Rosnay, P., Tavolato, C., Thepaut, J. N., Vitart, F.: The Era-Interim reanalysis: Configuration and performance of the data assimilation system, Q. J. R. Meteor. Soc. 137: 553–597, doi: 10.1002/qj.828, 2011.

Dee, D. P. and Uppala, S.: Variational bias correction of satellite radiance data in the ERA-Interim reanalysis. Q.J.R. Meteorol. Soc., 135: 1830-1841, doi: 10.1002/qj.493, 2009.

Dee, D. P., Balmaseda, M., Balsamo, G., Engelen, R., Simmons, A. J., and Thepaut, J.-N.: Towards a consistent reanalysis of the climate system, B. Am. Meteorol. Soc., 95, 1235–1248, doi:10.1175/BAMS-D-13-00043.1, 2014.

Dharssi, I., Steinle, P., and Candy, B.: Towards a Kalman filter based land surface data assimilation scheme for ACCESS, Bureau of Meteorology CAWCR Technical Report No. 54, http://www.cawcr.gov.au/technical-reports/CTR_054.pdf, 2012.

Dharssi, I., Steinle, P., and Fernon, J.: Improved numerical weather predictions by using optimised urban model parameter values and satellite derived tree heights. In Weber, T., McPhee, M.J. and Anderssen, R.S. (eds) MODSIM2015, 21st International Congress on Modelling and Simulation. Modelling and Simulation Society of Australia and New Zealand, December 2015, pp. 1161–1167. ISBN: 978-0-9872143-5-5. https://www.mssanz.org.au/modsim2015/M4/dharssi.pdf, 2015.

Dharssi, I., and Vinodkumar: JASMIN: A prototype high resolution soil moisture analysis system for Australia, Bureau of Meteorology Report No. 026, http://www.bom.gov.au/research/publications/researchreports/BRR-026.pdf, 2017.

Dickinson, R.E., Errico, R.M., Giorgi, F., and Bates, G. T.: A regional climate model for the western United States, 15: 383-422, doi: 10.1007/BF00240465, 1989.

Donlon, C. J., M. Martin, J. D. Stark, J. Roberts-Jones, E. Fiedler, and W. Wimmer: The Operational Sea Surface Temperature and Sea Ice analysis (OSTIA) system, Rem. Sens. Environ., 116, 140–158, doi: 10.1016/j.rse.2010.10.017, 2012.

Ebert, E.E., J.E. Janowiak, and C. Kidd: Comparison of near-real-time precipitation estimates from satellite observations and numerical models. Bull. Amer. Meteor. Soc., 88, 47–64, doi: 10.1175/BAMS-88-1-47, 2007.

Ebita, A., Kobayashi, S., Ota, Y., Moriya, M., Kumabe, R., Onogi, K., Harada, Y., Yasui, S., Miyaoka, K., Takahashi, K., Kamahori, H., Kobayashi, C., Endo, H., Soma, M., Oikawa, Y., and Ishimizu, T.: The Japanese 55-year reanalysis JRA-55: An interim report, SOLA, 7, 149–152, doi: 10.2151/sola.2011-038, 2011.

Evans, J. P., and McCabe, M. F.: Effect of model resolution on a regional climate model simulation over southeast Australia. Clim. Res., 56,131–145, doi: 10.3354/cr01151, 2013.

Fall, S., Niyogi, D., Gluhovsky, A., Pielke Sr, R. A., Kalnay, E., and Rochon, G.: Impacts of land use land cover on temperature trends over the continental United States: assessment using the North American Regional Reanalysis. Int. J. Climatol., 30, 1980-1993, doi: 10.1002/joc.1996, 2010.

Fowler, H. J., Blenkinshop, S., and Tebaldi, C.: Linking climate change modelling to impacts studies: recent advances in downscaling techniques for hydrological modeling. Int. J. Climatol. 27, 1547–1578, doi: 10.1002/joc.1556, 2007.

Franklin, C. N., Z. Sun, D. Bi, M. Dix, H. Yan, and A. Bodas-Salcedo: Evaluation of clouds in ACCESS using the satellite simulator package COSP: Global, seasonal, and regional cloud properties, J. Geophys. Res. Atmos., 118, 732–748, doi: 10.1029/2012JD018469, 2013.

Gauthier, P., and Thépaut, J.-N.: Impact of the digital filter as a weak constraint in the preoperational 4DVar assimilation system of Météo-France." Mon. Wea. Rev., 129, 2089-2102, doi: 10.1175/1520-0493(2001)129<2089:IOTDFA>2.0.CO;2, 2001.

Gelaro, R., W. McCarty, M. J. Suárez, R. Todling, A. Molod, L. Takacs, C. A. Randles, A. Darmenov, M. G. Bosilovich, R. Reichle, K. Wargan, L. Coy, R. Cullather, C. Draper, S. Akella, V. Buchard, A. Conaty, A.M. da Silva, W. Gu, G. Kim, R. Koster, R. Lucchesi, D. Merkova, J. E. Nielsen, G. Partyka, S. Pawson, W. Putman, M. Rienecker, S. D. Schubert, M. Sienkiewicz, and B. Zhao: The Modern-Era Retrospective Analysis for Research and Applications, Version 2 (MERRA-2), J. Clim., 30, 5419–5454, doi: 10.1175/JCLI-D-16-0758.1, 2017.

Gregory, D., and P. R. Rowntree: A mass flux convection scheme with representation of cloud ensemble characteristics and stability-dependent closure, Mon. Weath. Rev., 118, 1483–1506, doi: 10.1175/1520-0493(1990)118<1483:AMFCSW>2.0.CO;2, 1990.

Harris, B. A. and Kelly, G.: A satellite radiance-bias correction scheme for data assimilation. Q.J.R. Meteorol. Soc., 127: 1453-1468. doi:10.1002/qj.49712757418, 2001.

Hartmann, D. L., Klein Tank, A. M. G., Rusticucci, M., Alexander, L. V., Brönnimann, S., Charabi, Y., Dentener, F. J., Dlugokencky, E. J., Easterling, D. R., Kaplan, A., Soden, B. J., Thorne, P. W., Wild, M., and Zhai, P. M.: Observations: Atmosphere and Surface, in: Climate Change 2013: The Physical Science Basis. Contribution of Working Group I to the Fifth Assessment Report of the Intergovernmental Panel on Climate Change. Cambridge University Press, Cambridge, United Kingdom and New York, NY, USA, 2013.

Hersbach, H., and Dee, D.: ERA5 reanalysis is in production, ECMWF Newsletter No. 147, 7, accessed online https://www.ecmwf.int/sites/default/files/elibrary/2016/16299-newsletter-no147-spring-2016.pdf, 2016.

Holt, E., and Wang, J.: Trends in wind speed at wind turbine height of 80 m over the contiguous United States using the North American Regional Reanalysis (NARR), J. Appl. Meteor. Climatol., 51, 2188–2202, doi: 10.1175/JAMC-D-11-0205.1, 2012.

Howard, T., and Clark, P.: Correction and downscaling of NWP wind speed forecasts, Meteorol. Apps., 14, 105-116, doi: 10.1002/met.12, 2007.

Huffman, G. J., Adler, R. F., Bolvin, D. T., Gu, G., Nelkin, E. J., Bowman, K. P., Hong, Y., Stocker, E. F., and Wolff, D. B.: The TRMM multisatellite precipitation analysis (TMPA): Quasi-global, multiyear, combined-sensor precipitation estimates at fine scales, J. Hydrometeor., 8, 38–54, doi: 10.1175/JHM560.1, 2006.

Ingleby, N. B.: The statistical structure of forecast errors and its representation in The Met. Office Global 3-D variational data assimilation scheme. Q. J. R. Meteor. Soc. 127: 209-231, doi: 10.1002/qj.49712757112, 2001.

Jakob, D., Su, C.-H., Eizenberg, N., Kociuba, G., Steinle, P., Fox-Hughes, P., and Bettio, L.: An atmospheric high-resolution regional reanalysis for Australia, Bull. Aus. Meteor. Oceanog. Soc., 30, 16-23, 2017.

Jermey, P. M., and Renshaw, R. J.: Precipitation representation over a two-year period in regional reanalysis, Q. J. R. Meteorol. Soc., 142, 1300–1310, doi: 10.1002/qj.2733, 2016.

Jones, D. A., Wang, W., and Fawcett, R.: High-quality spatial climate data-sets for Australia, Aust. Meteorol. Oceanogr. J., 58, 233–248, 2009.

Kallberg, P.: Forecast drift in ERA-Interim. ERA report series 10, accessed online https://www.ecmwf.int/sites/default/files/elibrary/2011/10381-forecast-drift-era-interim.pdf, 2011.

Kalnay, E., M. Kanamitsu, R. Kistler, W. Collins, D. Deaven, L. Gandin, M. Iredell, S. Saha, G. White, J. Woollen, Y. Zhu, M. Chelliah, W. Ebisuzaki, W. Higgins, J. Janowiak, K.C. Mo, C. Ropelewski, J. Wang, A. Leetmaa, R. Reynolds, R. Jenne, and D. Joseph: The NCEP/NCAR 40-Year Reanalysis Project. Bull. Amer. Meteor. Soc., 77, 437–472, doi: 10.1175/1520-0477(1996)077<0437:TNYRP>2.0.CO;2, 1996.

Le Marshall, J., Xiao, Y., Norman, R., Zhang, K., Rea, A., Cucurull, L., Seecamp, R., Steinle, P., Puri, K., and Le, T.: The beneficial impact of radio occultation observations on Australian region forecasts, Aust. Meteorol. Oceanogr. J., 60:121–125, 2010.

Le Marshall, J., R. Seecamp, Y. Xiao, P. Gregory, J. Jung, P. Stienle, T. Skinner, C. Tingwell, and T. Le: The Operational Generation of Continuous Winds in the Australian Region and Their Assimilation with 4DVar. Wea. Forecasting, 28, 504–514, doi: 10.1175/WAF-D-12-00018.1, 2013.

Lean, H. W., Clark, P. A., Dixon, M., Roberts, N. M., Fitch, A., Forbes, R., and Halliwell, C.: Characteristics of high-resolution versions of the Met Office Unified Model for forecasting convection over the United Kingdom, Mon. Weath. Rev., 136, 3408–3424, doi: 10.1175/2008MWR2332.1, 2008.

Lorenc, A. C., and Hammon, O.: Objective quality control of observations using Bayesian methods. Theory, and a practical implementation. Q. J. Roy. Meteor. Soc., 114, 515-543, doi: 10.1002/qj.49711448012, 1988.

Lorenc, A. C.: Modelling of error covariances by 4D-Var data assimilation, Q. J. Roy. Meteor. Soc., 129, 3167–3182, doi: 10.1256/qj.02.131, 2003.

Lorenc, A. C., and Payne, T. J.: 4D-Var and the butterfly Effect: Statistical four-dimensional data assimilation for a wide range of scales, Q. J. Roy. Meteorol. Soc., 133, 607–614, doi: 10.1002/qj.36, 2007.

Loveland, T. R., B. C. Reed, J. F. Brown, D. O. Ohlen, Z. Zhu, L. Yang, and J. W. Merchant: Development of a global land cover characteristics database and IGBP DISCover from 1 km AVHRR data. Int. J. Rem. Sens., 21, 1303–1330, doi: 10.1080/014311600210191, 2000.

Ma, Y., Zhou, X., Bi, D., Sun, Z., and Hirst, A. C.: Improved air-sea flux algorithms in an ocean-atmosphere coupled model for simulation of global ocean SST and its tropical pacific variability, Clim. Dyn., 44, 1473–1485, doi: 10.1007/s00382-014-2281-7, 2015.

Mahmood, S., Davie, J., Jermey, P., Renshaw, R., George, J. P., Rajagopal, E. N., and Rani, S. I.: Indian monsoon data assimilation and analysis regional reanalysis: Configuration and performance, Atmos. Sci. Lett., 19, doi: 10.1002/asl.808, 2018.

Malloy, J.W., D.S. Krahenbuhl, C.E. Bush, R.C. Balling, M.M. Santoro, J.R. White, R.C. Elder, M.B. Pace, and R.S. Cerveny: A surface wind extremes ("wind lulls" and "wind blows") climatology for central North America and adjoining oceans (1979–2012). J. Appl. Meteor. Climatol., 54, 643–657, doi: 10.1175/JAMC-D-14-0009.1, 2015.

Martynov, A., Laprise, R., Sushama, L., Winger, K., Separovic, L., and Dugas, B.: Reanalysis-driven climate simulation over CORDEX North America domain using the Canadian Regional Climate Model, version 5: model performance evaluation. Clim. Dyn., 41, 2973-3005, doi: 10.1007/s00382-013-1778-9, 2013.

Masunaga, R., H. Nakamura, T. Miyasaka, K. Nishii, and Y. Tanimoto: Separation of climatological imprints of the Kuroshio Extension and Oyashio fronts on the wintertime atmospheric boundary layer: Their sensitivity to SST resolution prescribed for atmospheric reanalysis. J. Climate, 28, 1764−1787, doi: 10.1175/JCLI-D-14-00314.1, 2015.

Masunaga, R., Nakamura, H., Kamahori, H., Onogi, K., and Okajima, S.: JRA-55CHS: An atmospheric reanalysis produced with high-resolution SST, SOLA, 14, 6-13, doi: 10.2151/sola.2018-002, 2018.

Matthews, A. J., Pickup, G., Peatman, S.C., Clews, P., and Martin, J.: The effect of the Madden-Julian Oscillation on station rainfall and riverlevel in the Fly River System, Papua New Guinea, J. Geophys. Res. Atmos., 118, 10926–10935, doi:10.1002/jgrd.50865, 2013.

Mesinger, F., G. DiMego, E. Kalnay, K. Mitchell, P.C. Shafran, W. Ebisuzaki, D. Jović, J. Woollen, E. Rogers, E.H. Berbery, M.B. Ek, Y. Fan, R. Grumbine, W. Higgins, H. Li, Y. Lin, G. Manikin, D. Parrish, and W. Shi: North American Regional Reanalysis, Bull. Amer. Meteor. Soc., 87, 343–360, doi: 10.1175/BAMS-87-3-343, 2006.

Moore, R. J.: The PDM rainfall-runoff model. Hydrol. Earth Syst. Sci., 11: 483-499, doi: 10.5194/hess-11-483-2007, 2007.

Puri, K., G. Dietachmayer, P. Steinle, M. Dix, L. Rikus, L. Logan, M. Naughton, C. Tingwell, Y. Xiao, V. Barras, I. Bermous, R. Bowen, L. Deschamps, C. Franklin, J. Fraser, T. Glowacki, B. Harris, J. Lee, T. Le, G. Roff, A. Sulaiman, H. Sims, X. Sun, Z. Sun, H. Zhu, M. Chattopadhyay and C. Engel, Implementation of the initial ACCESS numerical weather prediction system. Aust. Meteorol. Oceanogr. J., 63, 265-284, 2013.

Radic, V., and Clarke, G. K. C.: Evaluation of IPCC models' performance in simulating late-twentieth-century climatologies and weather Patterns over North America. J. Climate, 24, 5257–5274, doi: 10.1175/JCLI-D-11-00011.1, 2011.

Ramella Pralungo, L., Haimberger, L., Stickler, A., and Brönnimann, S.: A global radiosonde and tracked balloon archive on 16 pressure levels (GRASP) back to 1905 – Part 1: Merging and interpolation to 00:00 and 12:00 GMT, Earth Syst. Sci. Data, 6, 185-200, doi: 10.5194/essd-6-185-2014, 2014.

Ramella Pralungo, L., and Haimberger, L.: A "Global Radiosonde and tracked-balloon Archive on Sixteen Pressure levels" (GRASP) going back to 1905 – Part 2: homogeneity adjustments for pilot balloon and radiosonde wind data, Earth Syst. Sci. Data, 6, 297-316, doi: 10.5194/essd-6-297-2014, 2014.

Rawlins, F., Ballard, S. P., Bovis, K. J., Clayton, A. M., Li, D., Inverarity, G. W., Lorenc, A. C., and Payne, T. J.: The Met Office global 4-dimensional data assimilation system. Q. J. Roy. Met. Soc., 133, 347–362, doi: 10.1002/qj.32, 2007.

Randall D. A., et. al., Climate models and their evaluation. In: climate change 2007: The physical science basis. Contribution of working group I to the fourth assessment report of the intergovernmental panel on climate change. In: Solomon, S., Qin, D., Manning, M., Chen, Z., Marquis, M., Averyt, K. B., Tignor, M., and Miller, H. L. (eds.) Cambridge University Press, Cambridge and New York, NY, 2007.

Renshaw, R., Jermey, P., Barker, D., Maycock, A., and Oxley, S.: EURO4M regional reanalysis system. Forecasting Research Technical Report No. 583, accessed online: https://www.metoffice.gov.uk/binaries/content/assets/mohippo/pdf/o/4/frtr583.pdf, 2013.

Roberts-Jones, J., E.K. Fiedler, and M.J. Martin: Daily, global, high-resolution SST and sea ice reanalysis for 1985–2007 Using the OSTIA system, J. Clim., 25, 6215–6232, doi: 10.1175/JCLI-D-11-00648.1, 2012.

Rose, S., and Apt, J.: Quantifying sources of uncertainty in reanalysis derived wind speed, Renewable Energy, 94, 157-165, doi: 10.1016/j.renene.2016.03.028, 2016.

Ruiz-Barradas, A. and Nigam, S.: IPCC's twentieth-century climate simulations: Varied representations of North American hydroclimate variability. J. Clim., 19, 4041–4058, doi: 10.1175/JCLI3809.1, 2006.

Sapiano, M. R. P., and Arkin, P. A.: An intercomparison and validation of high-resolution satellite precipitation estimates with 3-hourly gauge data, J. Hydrometeor., 10, 149-166, doi: 10.1175/2008JHM1052.1, 2009.

Sheridan, P., Smith, S., Brown, A., and Vosper, S.: A simple height-based correction for temperature downscaling in complex terrain, Meteor. App., 17, 329-339, doi: 10.1002/met.177, 2010.

Simard, M., N. Pinto, J. B. Fisher, and A. Baccini: Mapping forest canopy height globally with spaceborne lidar. J. Geophys. Res.: Biogeosci., 116, G04021, doi:10.1029/2011JG001708, 2011.

Walters, D., Boutle, I., Brooks, M., Melvin, T., Stratton, R., Vosper, S., et al.: The Met Office Unified Model Global Atmosphere 6.0/6.1 and JULES Global Land 6.0/6.1 configurations. Geosci. Model. Dev., 10, 1487–1520, doi: 10.5194/gmd-10-1487-2017, 2017a.

Walters, D., Baran, A., Boutle, I., Brooks, M., Earnshaw, P., Edwards, J., et al.: The Met Office Unified Model Global Atmosphere 7.0/7.1 and JULES Global Land 7.0 configurations. Geosci. Model Dev. Discuss., doi: 10.5194/gmd-2017-291, 2017b.

Wang, Z., Siems, S. T., Belusic, D., Manton, M. J., and Huang, Y.: A climatology of the precipitation over the Southern Ocean as observed at Macquarie Island. J. Appl. Meteorol. Climatol., 54, 2321-2337, doi: 10.1175/JAMC-D-14-0211.1

Wilson, D. R. and Ballard, S. P.: A microphysically based precipitation scheme for the UK Meteorological Office Unified Model, Q. J. R. Meteorol. Soc., 125, 1607–1636, doi:10.1002/qj.49712555707, 1999.

Wood, N., Staniforth, A., White, A., Allen, T., Diamantakis, M., Gross, M., Melvin, T., Smith, C., Vosper, S., Zerroukat, M., and Thuburn, J.: An inherently mass-conserving semi-implicit semi-Lagrangian discretization of the deep-atmosphere global non-hydrostatic equations, Q. J. R. Meteorol. Soc., 140, 1505–1520, doi:10.1002/qj.2235, 2014.

Zhao, M., Zhang, H-Q., and Dharssi, I.: Impact of land-surface initialization on ACCESS-S1 and comparison with POAMA. Bureau of Meteorology Research Report No. 023, Accessed online: http://www.bom.gov.au/research/publications/researchreports/BRR-023.pdf, 2017.

Zhu, H., and Dietachmayer, G.: Improving ACCESS-C convection settings, Bureau Research Report No. 008, Accessed online: http://www.bom.gov.au/research/publications/researchreports/BRR-008.pdf, 2015.

Zick, S. E., and Matyas, C. J.: Tropical cyclones in the North American Regional Reanalysis: An assessment of spatial biases in location, intensity, and structure, J. Geophys. Res.: Atmos., 120, 1651-1669, doi: 10.1002/2014JD022417, 2015.

Geosci. Model Dev. Discuss., https://doi.org/10.5194/gmd-2018-277
Manuscript under review for journal Geosci. Model Dev.
Discussion started: 6 December 2018

Geoscientific Model Development Discussions
Open Access
EGU

Figures

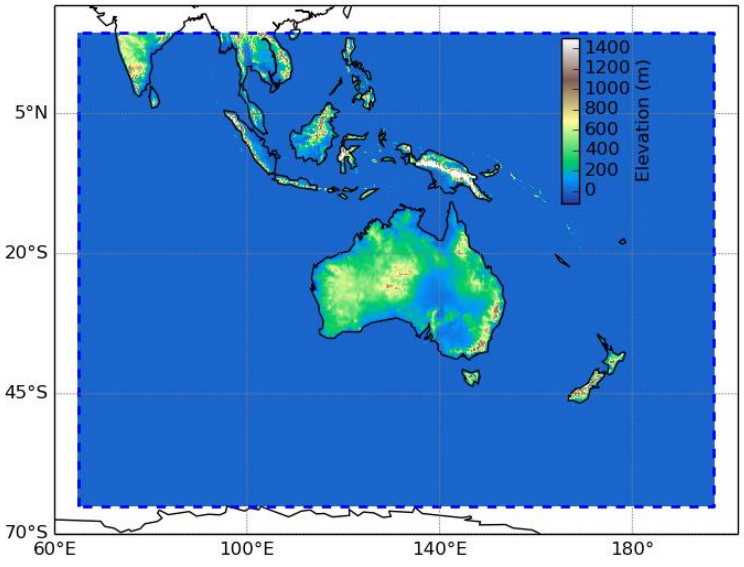

Figure 1 BARRA-R domain enclosed by the dashed box. Blue shading shows the model orography.

Geosci. Model Dev. Discuss., https://doi.org/10.5194/gmd-2018-277
Manuscript under review for journal Geosci. Model Dev.
Discussion started: 6 December 2018

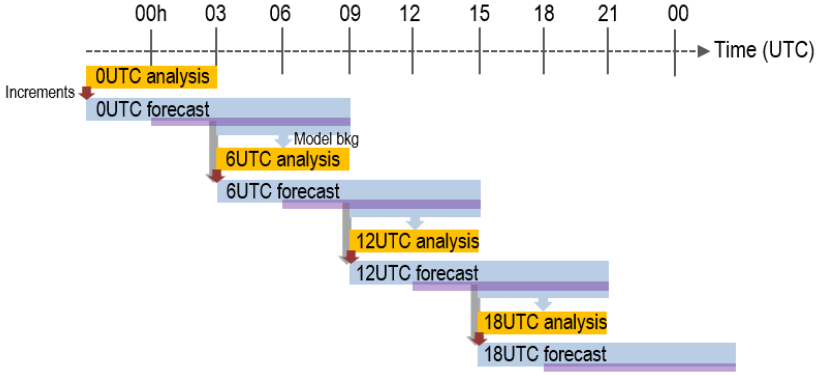

Figure 2 Cycling setup of BARRA-R at base time t_0 = 0, 6, 12, and 18 UTC. Each UM forecast is initialized at t_0-3h by the previous forecast (grey arrows) with increments from current analysis (red arrows). The purple bars indicate the time steps of the model states that have been archived.

Geosci. Model Dev. Discuss., https://doi.org/10.5194/gmd-2018-277
Manuscript under review for journal Geosci. Model Dev.
Discussion started: 6 December 2018

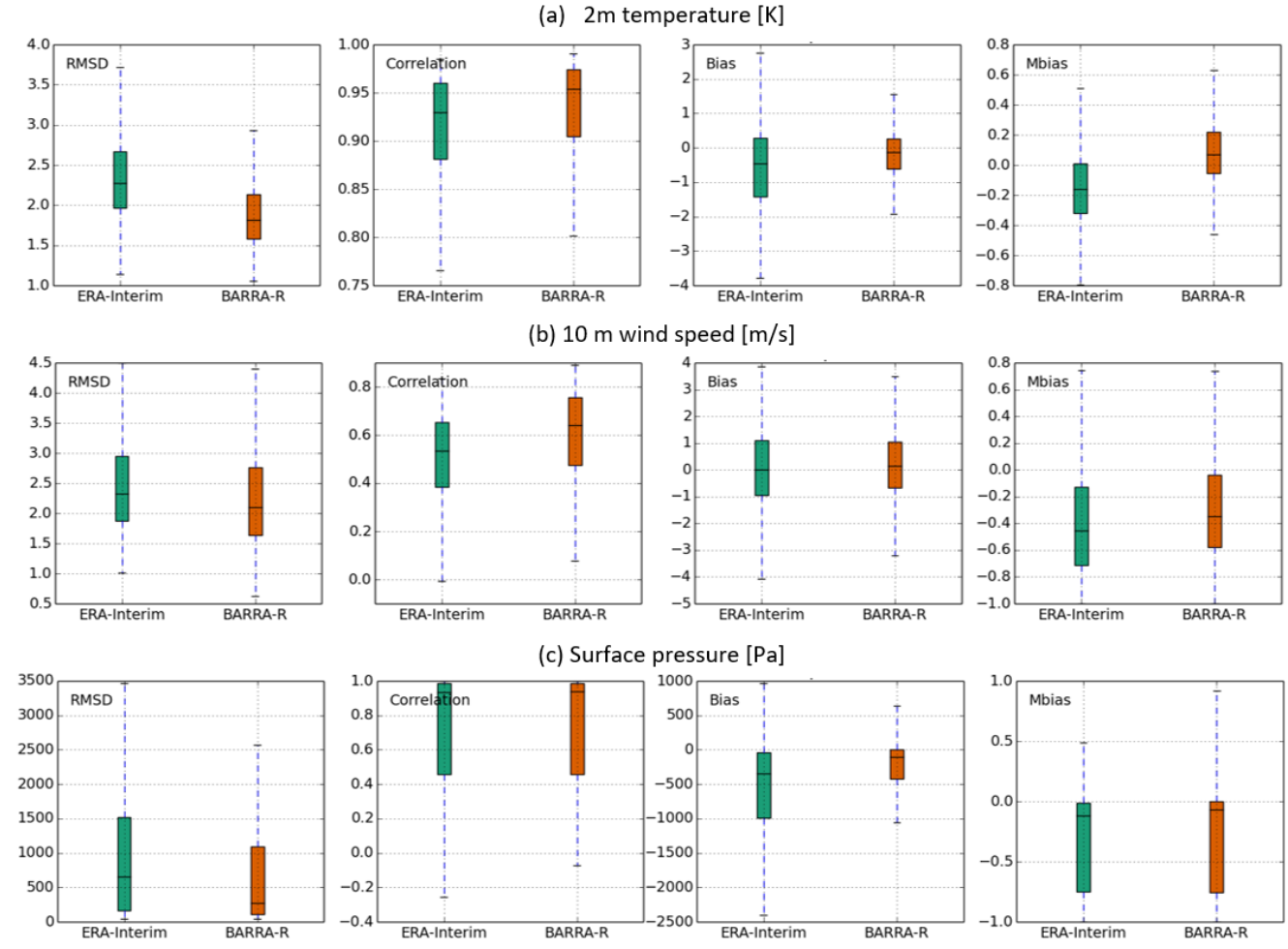

Figure 3 Boxplots showing the distribution of BARRA-R and ERA-Interim t_0+6h forecast scores over all stations in the BARRA-R domain. Individual boxes extend from first to third quartile. Medians are marked in each box and 'whiskers' cover the 5-95% percentile range.

Geosci. Model Dev. Discuss., https://doi.org/10.5194/gmd-2018-277
Manuscript under review for journal Geosci. Model Dev.
Discussion started: 6 December 2018

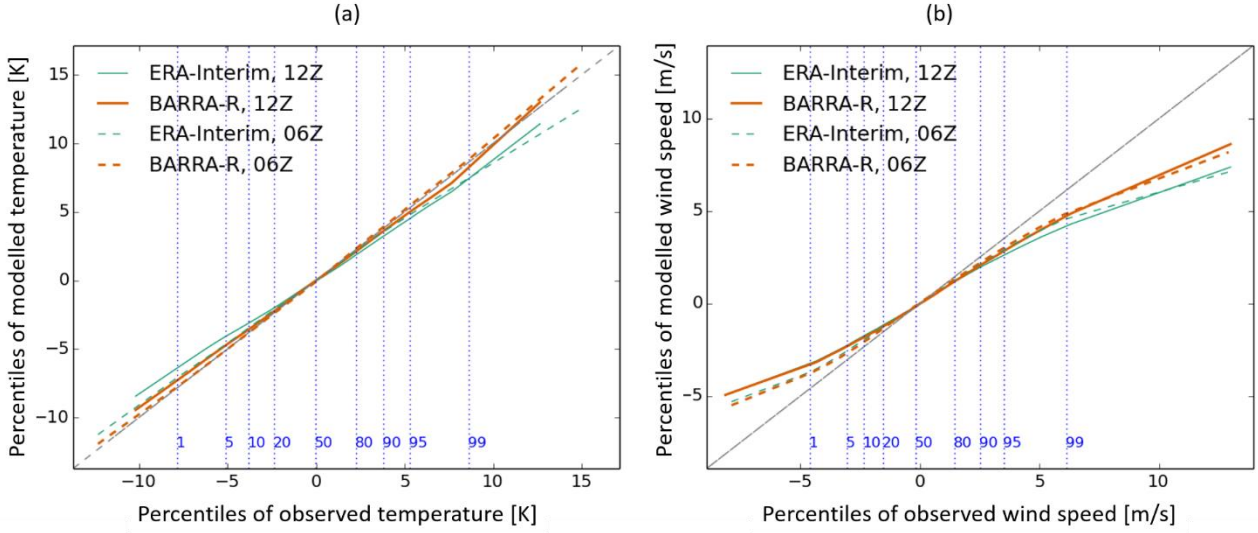

Figure 4 Comparisons of percentile values between observations and reanalyses for (a) 2 m temperature, and (b) 10 m wind speed during 2010. The values from 0.05% to 99.95% percentiles are calculated using values derived from monthly means. The vertical blue dashed lines indicate the corresponding percentiles of the observations.

Geosci. Model Dev. Discuss., https://doi.org/10.5194/gmd-2018-277
Manuscript under review for journal Geosci. Model Dev.
Discussion started: 6 December 2018

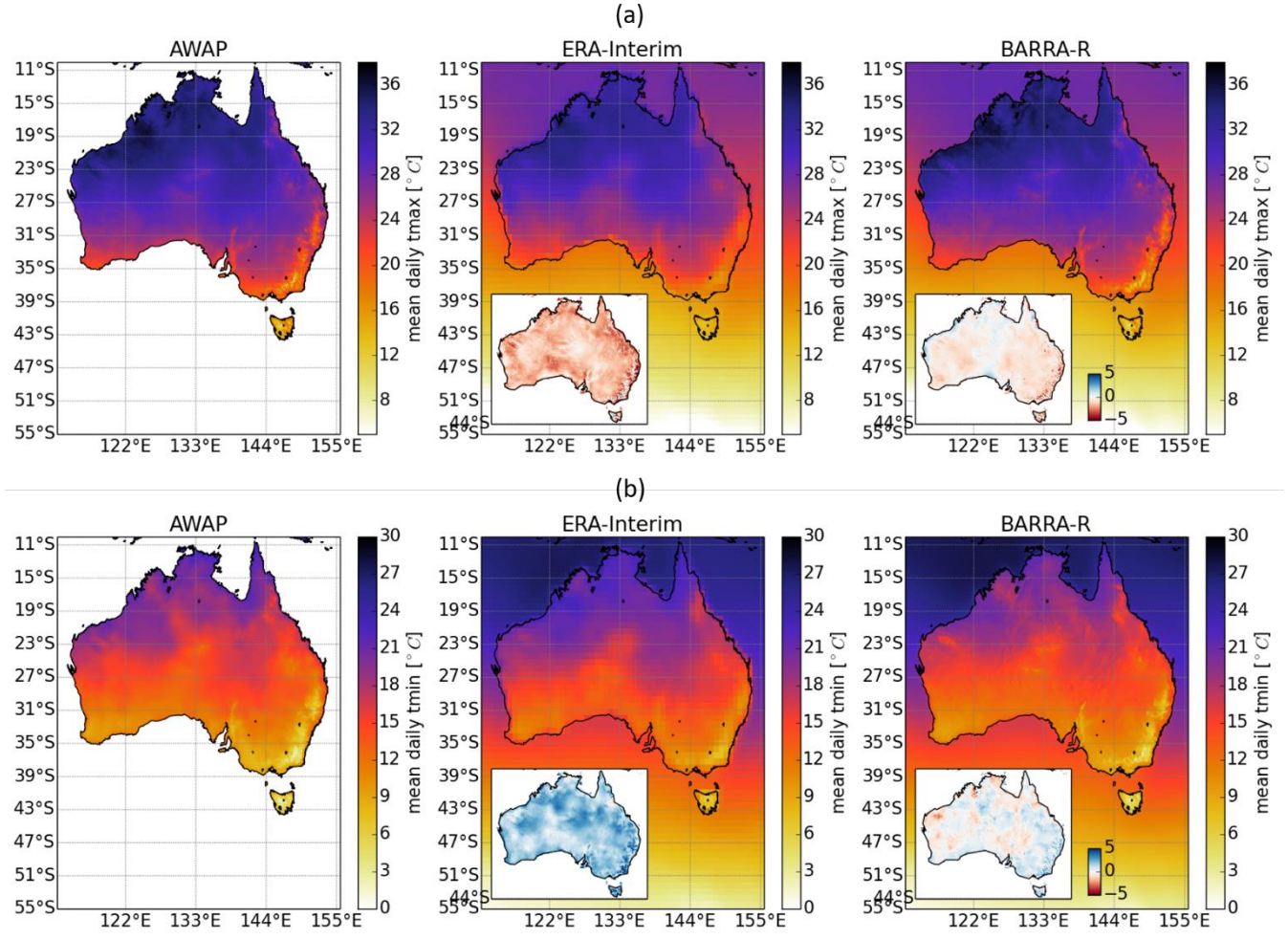

Figure 5 Mean daily minimum (top row) and maximum (bottom row) screen temperature from AWAP, ERA-Interim and BARRA-R. The insets show differences when subtracting AWAP statistic from the reanalyses.

Geosci. Model Dev. Discuss., https://doi.org/10.5194/gmd-2018-277
Manuscript under review for journal Geosci. Model Dev.
Discussion started: 6 December 2018

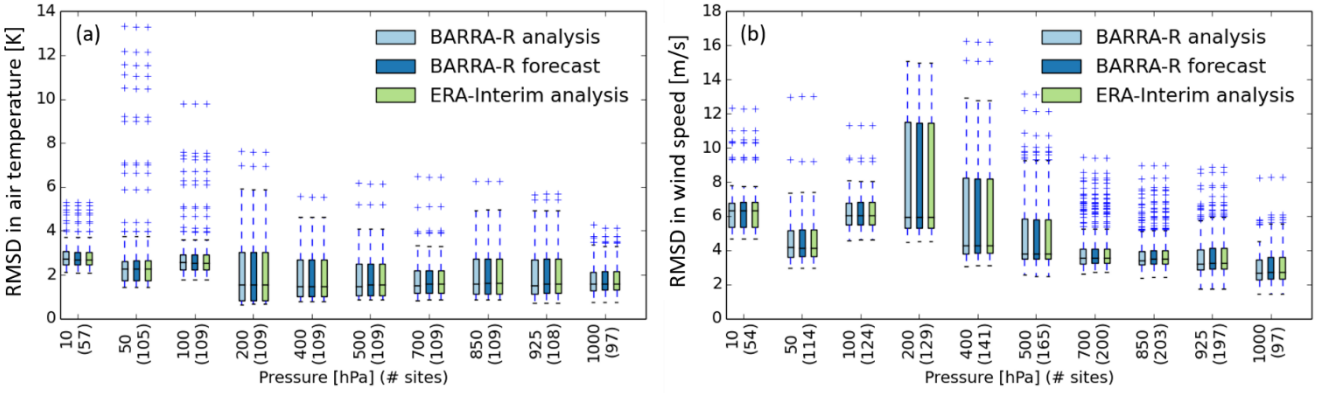

Figure 6 Boxplots showing the RMSD distribution of BARRA-R t_0+6 forecast and t_0 analysis, and ERA-Interim analysis for (a) temperature and (b) wind speed at over multiple sites in the BARRA-R domain. RMSD is calculated for temperature and wind speed at pressure levels 10, 50, 100, 200, 400, 500, 700, 850, 925 and 1000 hPa against pilot balloon and radiosonde observations at 0 and 12 UTC. The numbers of sites are indicated in the brackets.

Geosci. Model Dev. Discuss., https://doi.org/10.5194/gmd-2018-277
Manuscript under review for journal Geosci. Model Dev.
Discussion started: 6 December 2018

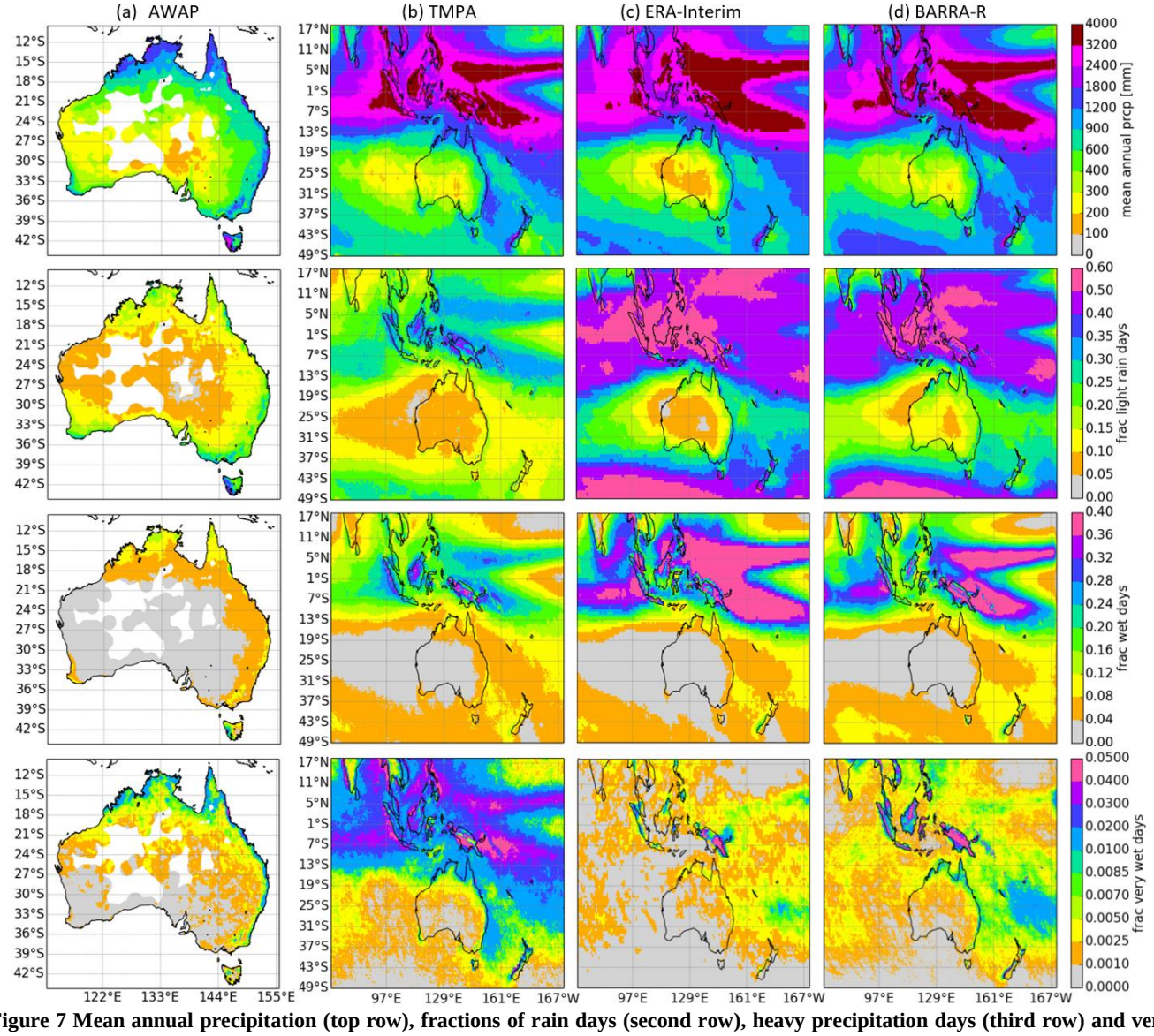

Figure 7 Mean annual precipitation (top row), fractions of rain days (second row), heavy precipitation days (third row) and very heavy precipitation days (bottom), from 2007 to 2016 from AWAP (first column), TMPA (second column), ERA-Interim (third column), and BARRA-R (last column). Regions with more than 10% missing values in AWAP are masked. Close ups of the plots over Australia are provided in the Supplementary Material.

Geosci. Model Dev. Discuss., https://doi.org/10.5194/gmd-2018-277
Manuscript under review for journal Geosci. Model Dev.
Discussion started: 6 December 2018

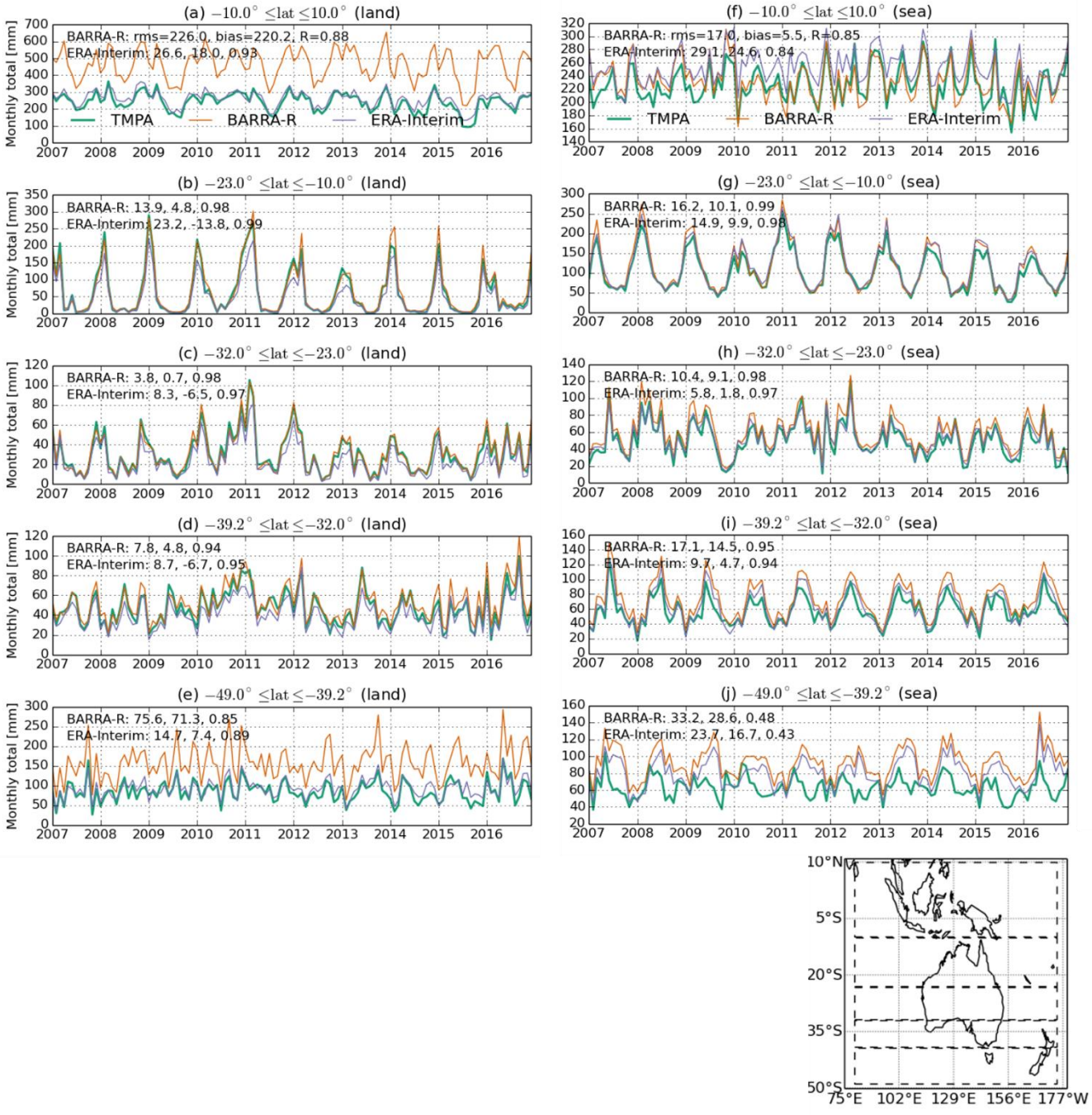

Figure 8 Monthly mean precipitation total [mm] over land (left) and sea (right), from TMPA, ERA-Interim and BARRA-R, in five sub-domains depicted in the inset. RMSD, bias and correlation are calculated between each reanalysis and TMPA.

Geosci. Model Dev. Discuss., https://doi.org/10.5194/gmd-2018-277
Manuscript under review for journal Geosci. Model Dev.
Discussion started: 6 December 2018

Geoscientific Model Development Discussions

Tables

Observations	Variables	Time periods	Sources
Land synoptic observations (LNDSYN)	Surface pressure, temperature, humidity, wind	1978-2017	Reanalysis prior to 2003 uses the data from ECMWF archive. Reanalysis between 2003 and 2009 uses the data from UKMO operational archive. Reanalysis from 2010 uses satellite data from the Bureau's operational archive. Bureau's archive also provides 10 minute land synoptic data from 2001, METARS between 2000 to 2009, TEMP from 2002 and WINPRO from 2010. New Zealand National Climate Database (CliDB) provides additional LNDSYN data over New Zealand.
Meteorological airfield reports (METARS)			
Ship synoptic observations (SHPSYN)			
Buoy	Surface pressure, temperature, wind		
Radiosondes (TEMP)	Upper-air wind, temperature, humidity	1978-2009	
Wind profilers (WINPRO)			
Wind-only sondes (PILOT)	Upper-air wind	1978-2017	
Aircraft Meteorological Data Relay (AMDAR)	Flight-level temperature, wind	1978-2017	
Air Report (AIREP)			
Advanced Infrared Sounder (AIRS)	Infrared radiances	2003-2017	
Advanced TIROS operational vertical sounder (ATOVS)	HIRS/AMSU radiances	1998-2017	
TIROS operational vertical sounder (TOVS)	MSU and HIRS radiances	1979-2002	
Infrared Atmospheric Sounding Interferometer (IASI)	Infrared radiances	2007-2017	
ESA Cloud motion winds (ESACMW)	Satellite radiometer-based winds (satwinds): cloud motion winds, AMV	1982-2017	
Geostationary Operational Environmental (GOESBUFR)		1995-2017	
Meteosat 2nd Generation satellite winds (MSGWINDS)		1982-2017	
Japanese Geostationary satellite winds (JMAWINDS)		1987-2017	
MODIS winds (MODIS)		2005-2017	
SeaWinds	Scatterometer-based winds (scatwinds)	1996-2009	
Advanced Scatterometer (ASCAT)		2007-2017	
GPS Radio Occultation (GPSRO)	Bending angle	2001-2017	Reanalysis prior to 2010 uses data provided by Radio Occultation Meteorology Satellite Application Facility (ROM SAF) archive, under EUMETSAT. Reanalysis from 2010 uses the data from the Bureau's operational archive.
Australian locally derived satwinds	AMV	2002-2017	Bureau of Meteorology operational archive
WindSat	Scatwinds	2015-2017	
Advanced Technology Microwave Sounder (ATMS)	Microwave radiances	2014-2017	
Cross-track Infrared Sounder (CrIS)	Infrared radiances	2014-2017	
Tropical Cyclone track (TCBOGUS)	Central pressure and position	1848-2016	International Best Track Archive for Climate Stewardship (IBTrACS)

Table 1 Observations assimilated in BARRA. Only the period concurrent with the reanalysis period is used. The various data sets were retrieved during the production, and thus the exact periods of each set used may differ.

Geosci. Model Dev. Discuss., https://doi.org/10.5194/gmd-2018-277
Manuscript under review for journal Geosci. Model Dev.
Discussion started: 6 December 2018

Geoscientific Model Development Discussions

	O-B		O-A	
Fields	**Bias**	**RMSD**	**Bias**	**RMSD**
Surface temperature (K)	-0.09	1.78	-0.10	1.61
Surface pressure (Pa)	-3.67	101.69	-2.08	68.85
Surface relative humidity (%)	0.0	10.0	0.00	8.0
Surface zonal wind (m/s)	0.05	1.97	-0.01	1.74
Surface meridional wind (m/s)	0.04	1.94	0.01	1.72
Aircraft potential temperature (K)	-0.24	1.34	-0.17	1.10
Aircraft zonal wind (m/s)	-0.04	3.05	-0.03	2.09
Aircraft meridional wind (m/s)	-0.18	3.06	-0.07	2.07
Sonde temperature at 980 hPa (K)	-0.15	1.11	-0.08	0.81
Sonde temperature at 500 hPa (K)	-0.33	0.92	-0.18	0.60
Sonde zonal wind at 980 hPa (m/s)	-0.15	2.45	-0.06	1.45
Sonde zonal wind at 500 hPa (m/s)	-0.17	2.52	-0.07	1.41
Sonde meridional wind at 980 hPa (m/s)	0.23	2.34	0.09	1.38
Sonde meridional wind at 500 hPa (m/s)	0.11	2.44	0.03	1.39
Satwind zonal wind (m/s)	0.36	3.16	0.27	2.72
Satwind meridional wind (m/s)	0.05	2.90	0.01	2.40
Scatwind zonal wind (m/s)	0.06	1.39	0.03	0.95
Scatwind meridional wind (m/s)	0.20	1.78	-0.02	1.32

Table 2 Comparisons of the 10-year mean of the RMSD and bias between the analyses and observations (O-A) and those between the background and observations (O-B), calculated for selected observational types across the BARRA-R domain. Values in green show reduction in the RMSD and the magnitude of the bias by the analyses, otherwise in red.